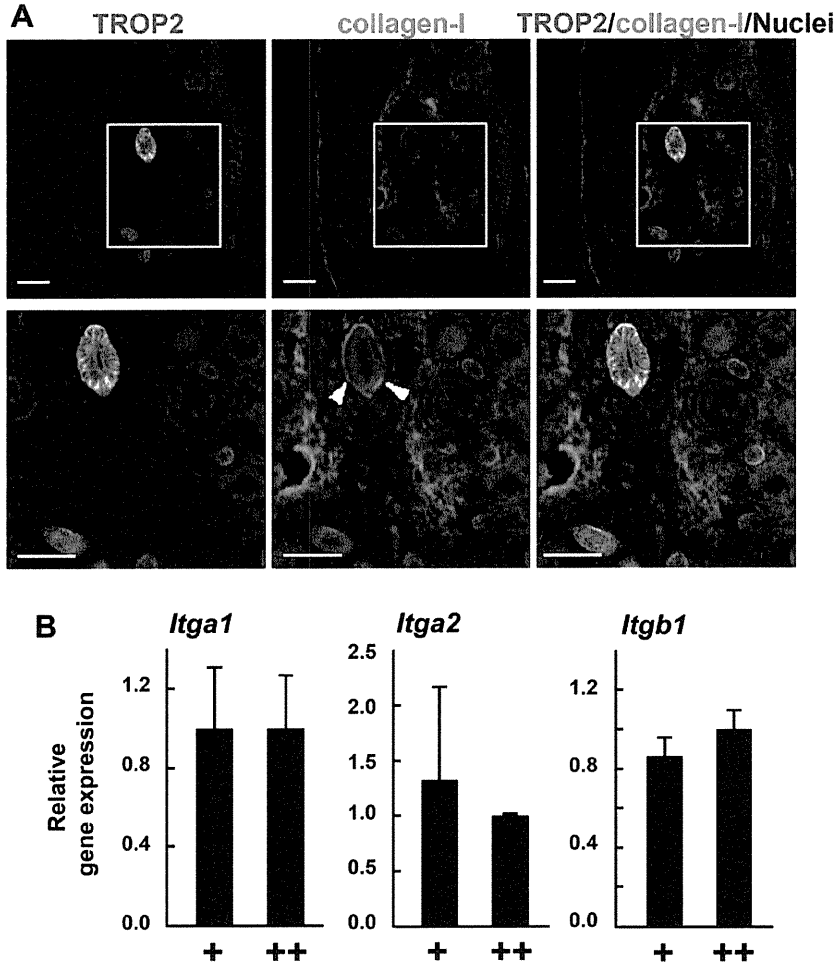

Figure 3. Expression of collagen-I and integrins in the fetal kidney. (A) Immunostaining of E14.5 kidney with anti-TROP2 (green) and anti-collagen-I (red) Abs and nuclei (blue). Higher magnification images of the boxed regions are shown underneath. Arrowheads indicate collagen-I surrounding the ureteric trunks. Scale bars = 100 μm. (B) Quantitative RT-PCR analysis of integrin subunits in freshly isolated EpCAM^{+}TROP2^{low}(+) and EpCAM^{+}TROP2^{high}(++) cells from E14.5 kidney. The relative gene expression of integrin/GAPDH is shown. Error bars are s.d.
doi:10.1371/journal.pone.0028607.g003

formation of branches of ureteric bud. As no endogenous canine TROP2 was detectable in MDCK cells by RT-PCR (Figure S4A), we established MDCK cell lines stably expressing TROP2 using retroviral vectors (Figure S4B and S4C).

To confirm the results obtained with the primary cultures of ureteric bud cells, the effect of TROP2 expression on the spreading of MDCK cells was examined. Cells detached from a confluent monolayer were plated on a collagen-coated glass cover slip and images were captured at 1 and 2.5 h after plating. Control MDCK cells started to spread at least 30 min earlier than MDCK-TROP2 cells (data not shown). At 2.5 h after plating, approximately 50% of the control MDCK cells had spread (Figure 5 A, B). By striking contrast, 70% of MDCK-TROP2 cells retained a round shape without cytoplasmic extensions. This result together with the results obtained using the primary cultures indicates that the expression of TROP2 significantly suppressed spreading of kidney cells.

MDCK cells displayed membrane ruffles with cortical actin filaments and stress fibers when cultured on collagen-coated glass cover slips, whereas TROP2 expression suppressed the membrane ruffling and stress fibers (Figure 5C). Since membrane ruffling is implicated in cell motility, we examined the effect of TROP2 on cell motility with the wound healing assay. The gap in cell sheets formed by a scratch was measured at 0 and 6 h. Expression of TROP2 suppressed the migration of MDCK cells 6 h after the scratch was made (Figure 5 D, E), suggesting that TROP2 also plays a role in suppressing cell spreading and migration on collagen.

TROP2 inhibits the branching of MDCK cells in collagen-gel culture

As the spreading and migration of ureteric bud cells are necessary for the development of renal tubules, we examined the effect of TROP2 on tubulogenesis and branch morphogenesis using MDCK cells in three-dimensional collagen-gel cultures. There was no significant difference in cyst size between clusters of control MDCK and MDCK-TROP2 cells in the collagen-gel cultures (Figure 6A, the top panels). The addition of 20 ng/mL of hepatocyte growth factor (HGF), a cell scattering factor, induced morphological changes in control MDCK cells, forming branches (Figure 6A, the left bottom panel). By contrast, MDCK-TROP2 cells formed round cysts without branching (Figure 6A, the right

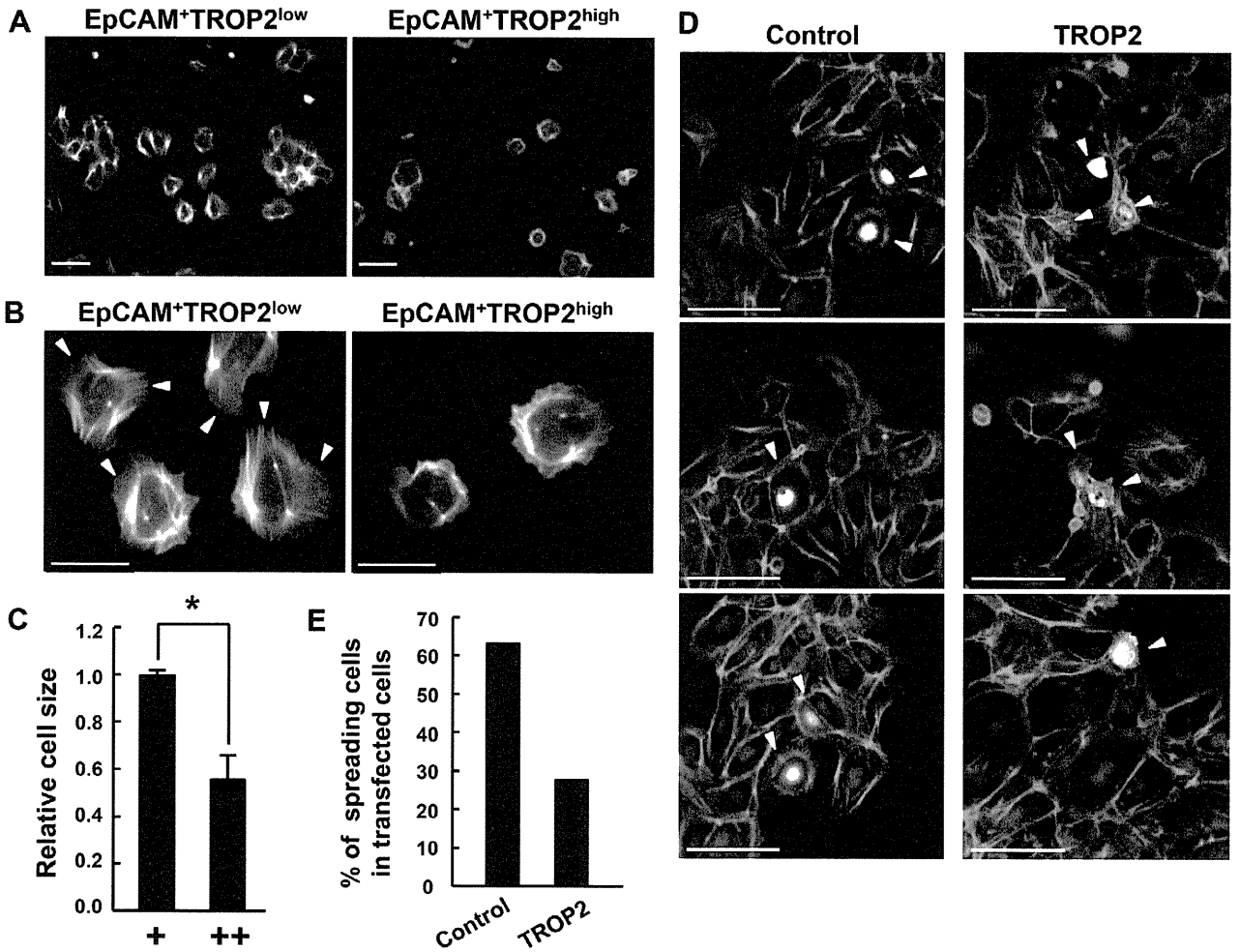

Figure 4. Characterization of ureteric tip and trunk cells in vitro. (A) Attachment of tip and trunk cells to collagen-coated plates. An equal number (5×10^3 cells/well) of freshly isolated EpCAM$^+$TROP2^{low} and EpCAM$^+$TROP2^{high} cells from E14.5 kidney were plated on a collagen-coated 96-well plate and stained for actin filaments with Alexa488-conjugated phalloidin (green) after 24 h of culture. The fluorescence of GFP and the actin filaments was visualized under a microscope. Nuclei (blue). Scale bars = 100 μm. (B) Cell morphology of ureteric bud tip and trunk cells. Higher-magnification images of (A) are shown. Arrowheads indicate the ruffles forming at the edge of membranes. Scale bars = 50 μm. (C) Spreading of EpCAM$^+$TROP2^{low}(+) and EpCAM$^+$TROP2^{high}(++) cells. Cell size was measured using imageJ (n = 3). Error bars are s.d., * $p<0.005$. (D) Cell morphology of EpCAM$^+$TROP2^{low} cells after enforced expression of TROP2. EpCAM$^+$TROP2^{low} cells cultured for 24 h were transiently transfected with pTIB741 or pTIB741-TROP2 plasmid. At 24 hours after transfection, cells were stained with Alexa555-phalloidin (red). Arrowheads indicate the transfected cells expressing GFP. (E) The ratio of spreading in transfected cells. The cell of which diameter is more than two-fold of nuclear is counted as "spreading cell". All the experiments were repeated three times and the similar results were obtained. Total number of tested transfectants is as follows: Control; 66, TROP2; 94. Representative results are shown.
doi:10.1371/journal.pone.0028607.g004

bottom panel) and ectopic TROP2 significantly suppressed the branching formation (Figure 6B). These results suggest that TROP2 antagonizes the cell scattering activity of HGF during branch formation. These results together reveal that TROP2 suppresses cell spreading and migration on collagen-I, suggesting that it contributes to the complicated branching structures of the kidney by suppressing the formation of branches from the ureteric bud trunks.

Discussion

TROP2 and EpCAM are structurally related molecules, however, their expression profiles differ significantly. In the E14.5 fetus, EpCAM is widely expressed in various epithelial tissues, whereas TROP2 expression is restricted to some epithelial cells in the kidney, lung and epidermis (Figure 1). During the branching morphogenesis of ureteric buds, new branches emerge from the tip through the proliferation and migration of tip cells. Meanwhile, the trunk elongates to form a rigid structure like a stalk without branching. TROP2 expression shows a gradient, increasing from the tip to trunk, suggesting that TROP2 contributes to the trunk structure (Figure 2).

ECM components play fundamental roles in the branching morphogenesis of the ureteric bud, exerting their functions through ECM-specific integrin receptors. Mice deficient in α3-integrin, a laminin-binding integrin subunit, fail to form branches of ureteric buds from the Wolffian duct, indicating laminin to be an important ECM component for branching morphogenesis [16]. On the other hand, the function of collagen-I in fetal kidney remains unknown, because mice deficient in either α1 or α2

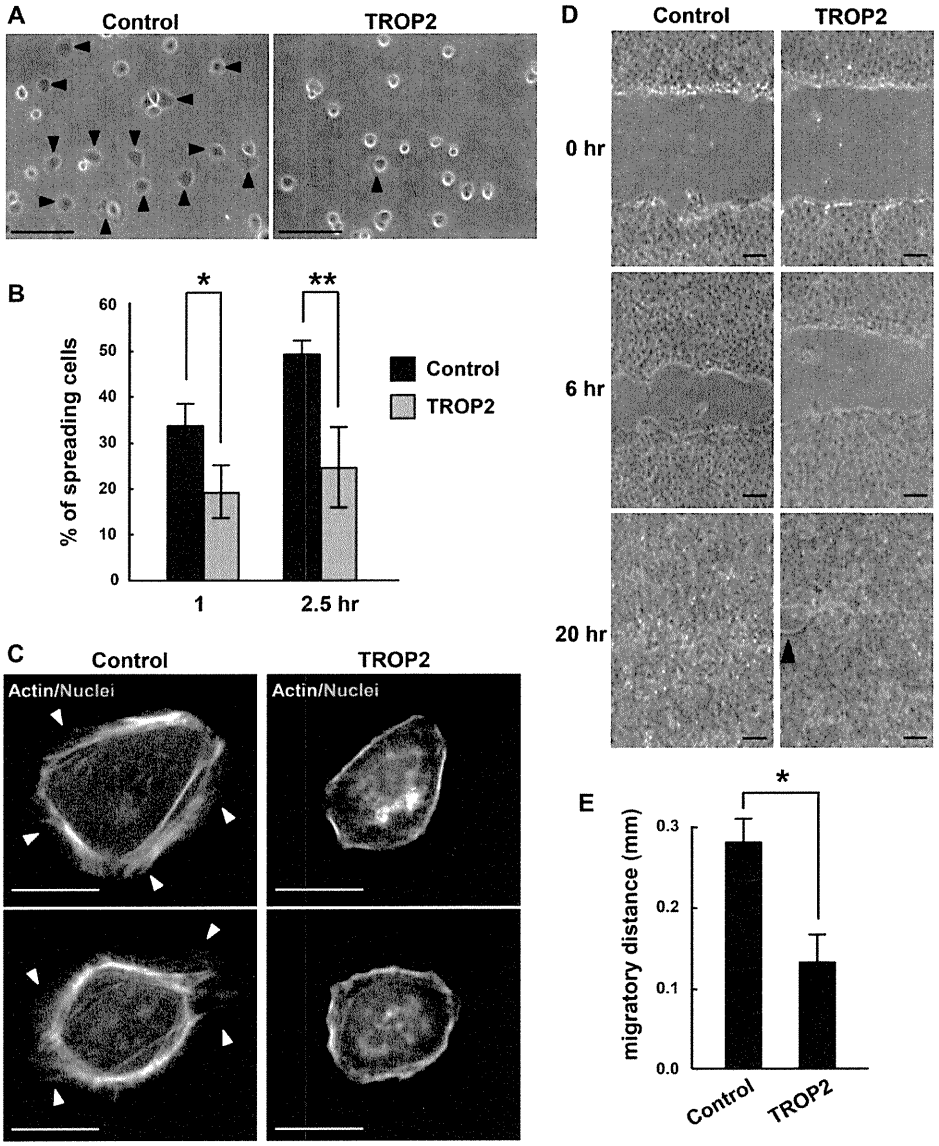

Figure 5. Attachment and migration of MDCK cells. (A) Cell spreading assay. Equal numbers of MDCK-control cells and MDCK-TROP2 cells, which expressed GFP and TROP2, respectively, were plated on collagen-coated glass coverslips. At 1 and 2.5 h after plating, spreading cells in several random fields were counted under a phase-contrast microscope. Arrowheads indicate spreading cells. Scale bars = 100 μm. (B) The percentage of spreading cells (n = 200). (C) MDCK-control cells and MDCK-TROP2 cells were plated on collagen-coated glass coverslips for 24 h and stained with Alexa555-Phalloidin. Arrowheads indicate the membrane ruffling at the edge of cells. Scale bars = 50 μm. (D) Wound healing assay. Cells grown as a monolayer on collagen-gel were scratched with a pipette tip. Photomicrographs were taken at 0, 6 and 16 h to record the healing process. Representative images are shown. An arrowhead indicates the unrecovered area. Scale bars = 100 μm. (E) The average migratory distance at 6 h after the scratch was measured manually (n = 3). Error bars, s.d. * $p<0.05$, ** $p<0.01$.
doi:10.1371/journal.pone.0028607.g005

collagen-I-binding integrin subunit do not show severe defects in the branching of ureteric buds [35,36]. However, collagen-gel cultures of MDCK cells show that integrin α1 and α2 are essential for generating new branches and tubular structures [30,37]. We have demonstrated here that collagen-I is present around the ureteric bud and there is a gradient of its expression from the tip to trunk during branching (Figure 3 and Figure S3). These results together suggest that collagen-I plays an important role in branching morphogenesis in fetal kidney.

An important finding of this study is the restricted expression and co-localization of TROP2 and collagen-I at the trunk of the ureteric duct. In contrast to collagen-I, where expression is restricted to that region, laminin is expressed almost uniformly around the ureteric bud (Figure S5). These expression patterns suggest a functional link between TROP2 and collagen-I. In fact, $TROP2^{high}$ trunk cells showed reduced adhesion and spreading on collagen-I-coated plates compared to $TROP2^{low}$ tip cells, though levels of collagen-binding integrin receptors α1, α2 and β1 were comparable between the trunks and tips (Figure 3B). To reveal the role in TROP2 for the binding and spreading of ureteric bud cells on collagen-I, we overexpressed TROP2 in $TROP2^{low}$ tip cells and found the binding and spreading to be reduced. We also demonstrated that TROP2 expression inhibits the spreading and migration of MDCK cells on collagen-I.

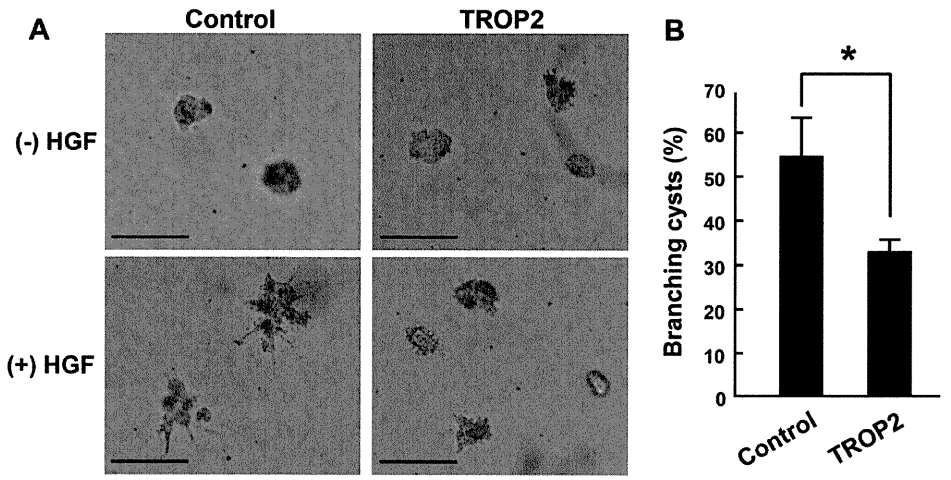

Figure 6. Branch formation in collagen-gel culture of MDCK cells. (A) Phase-contrast images of MDCK-control cells and MDCK-TROP2 cells cultured in 3-dimensional collagen gels. The cells were cultured without (upper panels) or with 20 ng/mL of HGF (lower panels). Both cells proliferated and formed round cysts without HGF (upper panels). Branches were formed in MDCK-control cells but suppressed in MDCK-TROP2 cells (lower panels). Scale bars = 100 μm. (B) The percentage of branching cysts in the culture with HGF. (n = 3). Error bars, s.d. * $p<0.05$.
doi:10.1371/journal.pone.0028607.g006

Branching morphogenesis is regulated by not only the ECM but also growth factor signaling. In collagen-gel cultures of MDCK cells, a well-established model of branch formation, growth factors such as HGF and GDNF are necessary for branching [18,38]. Studies with fetal kidney organ cultures and knockout mice have revealed the essential roles for many growth factors in branching morphogenesis. In response to growth factors, tip cells proliferate, migrate and finally form new branches, whereas trunk cells exhibit cell polarization, elongation and anti-apoptotic activity without branching [39–41]. In this paper we showed that TROP2 inhibits not only the attachment of cells onto collagen-coated plates but also branching in collagen-gel cultures. These results strongly suggest that TROP2 suppresses the formation of new branches at the trunk of the ureteric bud.

Focal adhesion kinase (Fak) is phosphorylated by the activation of integrins through binding to ECM and also growth factor stimulation [42]. p-Fak promotes cell extension and migration through actin polymerization and the connection of F-actin to integrin and growth factor receptors at the edge of cells, contributing to branching. In cell spreading assays, the phosphorylation level of Fak in MDCK-TROP2 cells was declined (Figure S6A), suggesting that TROP2 may inhibit the Fak signaling pathway at the ureteric trunk to avoid extra branching. While immunostaining showed that p-FAK levels are comparable in the tip and trunk cells (Figure S6B), it may be difficult to capture the transient event in static sections.

TROP2 and EpCAM are expressed in normal epithelial tissues, while they are known as oncogene and promote cancer cell proliferation and migration. EpCAM up-regulates cell motility by binding to several membrane proteins, Claudins, CD44 and tetraspanins, and α-actinin, a linker of F-actins [8,43]. Furthermore, in cancer cells, intracellular domain of EpCAM cleaved by TACE and presenilin-2 accelerates cell proliferation through the activation of β-catenin signaling [9]. By contrast, the molecular mechanisms of TROP2 in normal and cancer tissue are not known. Immunoprecipitation assays showed that TROP2 binds EpCAM (data not shown), suggesting the possibility that TROP2 interacts with EpCAM and regulates the cell proliferation and migration activity. In ureteric bud development, TROP2 expression shows a gradient pattern in contrast to uniform expression of EpCAM. Furthermore, the TROP2 expression declines toward tip where cells are actively proliferating and migrating, suggesting that TROP2 is involved in regulation of cell proliferation, possibly via interaction with other proteins like EpCAM. Thus, the difference in expression profiles of TROP2-interacting proteins between normal and cancer cells may modulate the function of TROP2. The precise role of the TROP2 in normal and cancer tissue needs further investigation.

In the lung, which also has a tree-like structure, branching morphogenesis is induced by the interaction between mesenchyme and epithelial cells, similar to the ureteric bud [44]. However, TROP2 is not expressed in the lung (Figure 1A) and the branching pattern is clearly different from the ureteric buds in the early stages. Lung epithelial cells generate several lateral branches from trunks. By contrast, the ureteric bud generates two epithelial tips after the first branching and repeats this dichotomous branching process, and trunks form a rigid duct structure by establishing tight cell-cell junctions and suppressing the formation of new branches [45]. Specific expression of TROP2 in the kidney may result in the difference in branching patterns between the lung and kidney.

In conclusion, this study revealed a unique pattern of TROP2 expression in the ureteric bud, i.e., the expression was strongest in the trunk and gradually declined toward the tip. TROP2 and collagen-I were co-localized to the basal membrane of the trunk cells and TROP2 suppressed cell spreading and migration on collagen-I. Based on these findings, we propose that TROP2 plays a role in the morphogenesis of the ureteric bud by inhibiting unnecessary branching from the trunk. Further studies on the function of TROP2 forming a specific pattern of tubular structures should shed light on the molecular basis of branching in various organs.

Materials and Methods

Ethics Statement

The mice were maintained and mated in the institutional animal facility according to the guidelines of the University of Tokyo. The experimental procedures in this study were approved by the Animal Research Committee of the Institute of Molecular and Cellular Biosciences, the University of Tokyo (approval number is 23003).

Immunohistochemistry

Mouse embryonic kidneys were fixed for 16 h at 4°C in Zamboni's solution [46], which was replaced with a 10, 15 and

finally 20% sucrose solution at 4°C for 12 h, respectively. They were embedded in OCT compound and frozen. Thin sections were prepared with a cryostat (Leica). Cultured ureteric bud cells and MDCK cells were fixed in 4% PFA for 10min. Samples were incubated with the primary antibodies listed in Table S1. Signals were visualized with Alexa Fluor-conjugated secondary antibodies (Molecular Probes) used at a dilution of 1:500. F-actin bundles were detected with Alexa Fluor 488- or 555-conjugated phalloidin (Molecular Probes) at a dilution of 1:250. Nuclei were counterstained with Hoechst 33342 (Sigma).

Flow cytometric analysis and cell sorting

Kidneys isolated from embryos were incubated with 0.25% trypsin and 0.5mM EDTA at 37°C for 30min and dissociated into a single-cell suspension. Cells were co-stained with fluorescein- and biotin-conjugated antibodies, washed, incubated with allophycocyanin-conjugated streptavidin (Invitrogen), and analyzed by FACSCalibur (Becton Dickinson). Dead cells were excluded by propidium iodide staining. For cell sorting, MoFlo XDP (Beckman Coulter) was used.

RNA extraction and quantitative reverse transcription PCR (RT-PCR)

Total RNA was extracted from each cell preparation using a First Pure RNA kit (Takara). Total RNA (0.3 μg) and random hexamer primers were used to synthesize cDNA with a High Capacity cDNA Reverse Transcription Kit (Applied Biosystems). Quantitative Real-time RT-PCR experiments were conducted with a LightCycler (Roche Diagnostics) and SYBR Premix Ex Taq (Takara-bio). Primers for Glyceraldehyde-3-phosphate dehydrogenase (Gapdh) were used as the control. The pairs of primers used were as follows: 5′-TGAACGGGAAGTCACTGG-3′ (*Gapdh* primer, sense), 5′-TCCACCACCCTGTTGCTGTA-3′ (*Gapdh* primer, antisense), 5′-CTGACCTAGACTCCGAGCTG-3′ (*TROP2* primer, sense), 5′-CGGCCCATGAACAGTGACTC-3′ (*TROP2* primer, antisense), 5′-AGGGGCGATCCAGAACAACG-3′ (*EpCAM* primer, sense), 5′-ATGGTCGTAGGGGCTTTCT-3′ (*EpCAM* primer, antisense), 5′-AAGTACAGCACCAAGTTCCTCAGC-3′ (*Wnt9b* primer, sense), 5′-GAACAGCACAGGAGCCTGACAC-3′ (*Wnt9b* primer, antisense), 5′-CTGAATCAGACGCAACACTG-TAAAC-3′ (*Wnt11* primer, sense), 5′-CTCTCTCCAGGTCAAG-CAGGTAG-3′ (*Wnt11* primer, antisense), 5′-GGAAGGT-GTCGTTGATGAAGGA-3′ (*Ret* primer, sense), 5′-CTCAGCA-TCCGCAATGGTG-3′ (*Ret* primer, antisense), 5′-CACTCCTG-GATTTGCTGATGT-3′ (*GFRα* primer, sense), 5′-CTGAAG-TTGGTTTCCTTGCCC-3′ (*GFRα* primer, antisense), 5′-CCC-GATGACCAAATGAAAGACG-3′ (*Sall1* primer, sense), 5′-TA-GAGAGGTTGTGATCGCTGA-3′ (*Sall1* primer, antisense).

Culture of ureteric bud cells and transfections

Ureteric bud cells from E14.5 kidneys were suspended in DMEM/F12 (1:1) medium (Gibco) containing 10% FBS (JRH) and antibiotics. Cells were seeded on type-I collagen-coated dishes. Relative cell size was measured as the actin-positive area using ImageJ (Rasband, W.S., NIH) and cellular area was determined. To express mouse TROP2, its cDNA fragment was inserted upstream of IRES-GFP in the vector pTIB731, provided by Dr. Tohru Itoh (University of Tokyo). Ureteric bud cells were sorted and cultured for 24 h prior to transfection. The transfection was carried out using polyethyleneimine "Max" reagent (Polysciences Inc.). Twenty four hours later, the cells were immunostained and the size of the GFP^+ transfected cells was examined under a fluorescence microscope.

MDCK cell culture and virus infection

MDCK cells were cultured in DMEM (Gibco) containing 10% FBS (Equitech) and antibiotics [34]. For expression of mouse TROP2, its cDNA was inserted into the pMxs vector. The pMxs-IRES-GFP vector was used as a negative control. Retrovirus was produced using the retrovirus packaging cell line PLAT-A and MDCK cells were infected as described previously [47]. Cells expressing TROP2 or GFP were sorted using anti-TROP2 Abs or GFP and MDCK cells expressing GFP (MDCK-control) or TROP2 (MDCK-TROP2) were established.

Immunoblotting

MDCK cells were lysed in TNE buffer (20 mM Tris-HCl, pH 7.4, 150 mM NaCl, 2 mM EDTA, 1% Nonidet P-40, 1 mM phenylmethylsulfonyl fluoride, 1 mM Pefabloc SC (Roche Applied Science), and 10 μg/ml leupeptin), and the whole cell extracts were separated by SDS-PAGE and transferred onto polyvinylidene difluoride membranes (Immobilon-P; Millipore). The membranes were subjected to Western blot analyses with anti-TROP2, anti-Fak or anti-p-Fak (Tyr397) antibody. Anti-β-actin antibody was used to confirm equal loadings.

Cell spreading assay

MDCK cells were detached by trypsin and resuspended in serum-free medium at 5×10^3 cells/ml. The cell suspension (1 ml) was added to type I collagen-coated coverslips. Cells were allowed to spread, and spread cells were scored manually under a phase-contrast microscope at 1 and 2.5 h after plating. Spread cells were defined as the cells with extended processes.

Wound healing assay

MDCK cells were grown on collagen-coated 60 mm dishes. The monolayer of cells was scratched with a pipette tip and the culture medium was changed to serum-free medium. Pictures were taken at 0, 6 and 16 h and the length of the gap between cell sheets was measured at 0 and 6 h.

Collagen gel culture

MDCK cells were detached from plates with trypsin and triturated into a single cell suspension. Cells were diluted to 0.5×10^3 cells/mL in a type I collagen solution and the cell solution was plated in a 24-well plate (500 μL/well). After incubation at 37°C to allow the collagen solution to gel, 1 mL of the culture medium was added. The medium was changed every 24 h, and after 2 days, medium containing 20 ng/mL of HGF was added and cultured for additional 2 days.

Supporting Information

Figure S1 Expression of TROP2 and Ki67 in E14.5 kidney.
(TIF)

Figure S2 Expression of Claudin7 and TROP2 in E14.5 kidney.
(TIF)

Figure S3 Expression of collagen-I and EpCAM in E14.5 kidney.
(TIF)

Figure S4 Establishment of MDCK cells expressing TROP2.
(TIF)

Figure S5 Expression of laminin in E14.5 kidney.
(TIF)

Figure S6 Phosphorylated-FAK in the tip and trunk of the ureteric bud.
(TIF)

Table S1 Primary antibodies used in immunofluorescence chemistry and flow cytometric analysis.
(TIF)

Acknowledgments

We thank Dr. Naoki Tanimizu for the critical reading of the manuscript. We also thank Drs. Tohru Itoh and Shiro Suetsugu for their valuable advice and providing reagents, and Nahoko Miyata and Shigeru Saito for technical assistance.

Author Contributions

Conceived and designed the experiments: YT MT AM. Performed the experiments: YT. Analyzed the data: YT. Contributed reagents/materials/analysis tools: YT MT AM. Wrote the paper: YT MT AM.

References

1. Cubas R, Li M, Chen C, Yao Q (2009) Trop2: a possible therapeutic target for late stage epithelial carcinomas. Biochim Biophys Acta 1796: 309–314.
2. Yagel S, Shpan P, Dushnik M, Livni N, Shimonovitz S (1994) Trophoblasts circulating in maternal blood as candidates for prenatal genetic evaluation. Hum Reprod 9: 1184–1189.
3. Goldstein AS, Lawson DA, Cheng D, Sun W, Garraway IP, et al. (2008) Trop2 identifies a subpopulation of murine and human prostate basal cells with stem cell characteristics. Proc Natl Acad Sci U S A 105: 20882–20887.
4. Okabe M, Tsukahara Y, Tanaka M, Suzuki K, Saito S, et al. (2009) Potential hepatic stem cells reside in EpCAM+ cells of normal and injured mouse liver. Development 136: 1951–1960.
5. El Sewedy T, Fornaro M, Alberti S (1998) Cloning of the murine TROP2 gene: conservation of a PIP2-binding sequence in the cytoplasmic domain of TROP-2. Int J Cancer 75: 324–330.
6. Litvinov SV, Balzar M, Winter MJ, Bakker HA, Briaire-de Bruijn IH, et al. (1997) Epithelial cell adhesion molecule (Ep-CAM) modulates cell-cell interactions mediated by classic cadherins. J Cell Biol 139: 1337–1348.
7. Munz M, Kieu C, Mack B, Schmitt B, Zeidler R, et al. (2004) The carcinoma-associated antigen EpCAM upregulates c-myc and induces cell proliferation. Oncogene 23: 5748–5758.
8. Nubel T, Preobraschenski J, Tuncay H, Weiss T, Kuhn S, et al. (2009) Claudin-7 regulates EpCAM-mediated functions in tumor progression. Mol Cancer Res 7: 285–299.
9. Maetzel D, Denzel S, Mack B, Canis M, Went P, et al. (2009) Nuclear signalling by tumour-associated antigen EpCAM. Nat Cell Biol 11: 162–171.
10. Maghzal N, Vogt E, Reintsch W, Fraser JS, Fagotto F (2010) The tumor-associated EpCAM regulates morphogenetic movements through intracellular signaling. J Cell Biol 191: 645–659.
11. Wang J, Day R, Dong Y, Weintraub SJ, Michel L (2008) Identification of Trop-2 as an oncogene and an attractive therapeutic target in colon cancers. Mol Cancer Ther 7: 280–285.
12. Nakatsukasa M, Kawasaki S, Yamasaki K, Fukuoka H, Matsuda A, et al. (2010) Tumor-associated calcium signal transducer 2 is required for the proper subcellular localization of claudin 1 and 7: implications in the pathogenesis of gelatinous drop-like corneal dystrophy. Am J Pathol 177: 1344–1355.
13. Costantini F, Kopan R (2010) Patterning a complex organ: branching morphogenesis and nephron segmentation in kidney development. Dev Cell 18: 698–712.
14. Dressler GR (2006) The cellular basis of kidney development. Annu Rev Cell Dev Biol 22: 509–529.
15. De Arcangelis A, Mark M, Kreidberg J, Sorokin L, Georges-Labouesse E (1999) Synergistic activities of alpha3 and alpha6 integrins are required during apical ectodermal ridge formation and organogenesis in the mouse. Development 126: 3957–3968.
16. Kreidberg JA, Donovan MJ, Goldstein SL, Rennke H, Shepherd K, et al. (1996) Alpha 3 beta 1 integrin has a crucial role in kidney and lung organogenesis. Development 122: 3537–3547.
17. Michael L, Davies JA (2004) Pattern and regulation of cell proliferation during murine ureteric bud development. J Anat 204: 241–255.
18. Chi X, Michos O, Shakya R, Riccio P, Enomoto H, et al. (2009) Ret-dependent cell rearrangements in the Wolffian duct epithelium initiate ureteric bud morphogenesis. Dev Cell 17: 199–209.
19. Costantini F, Shakya R (2006) GDNF/Ret signaling and the development of the kidney. Bioessays 28: 117–127.
20. Trzpis M, Popa ER, McLaughlin PM, van Goor H, Timmer A, et al. (2007) Spatial and temporal expression patterns of the epithelial cell adhesion molecule (EpCAM/EGP-2) in developing and adult kidneys. Nephron Exp Nephrol 107: e119 131.
21. Tsuzuki T, Takahashi M, Asai N, Iwashita T, Matsuyama M, et al. (1995) Spatial and temporal expression of the ret proto-oncogene product in embryonic, infant and adult rat tissues. Oncogene 10: 191–198.
22. Pachnis V, Mankoo B, Costantini F (1993) Expression of the c-ret proto-oncogene during mouse embryogenesis. Development 119: 1005–1017.
23. Kispert A, Vainio S, Shen L, Rowitch DH, McMahon AP (1996) Proteoglycans are required for maintenance of Wnt-11 expression in the ureter tips. Development 122: 3627–3637.
24. Enomoto H, Araki T, Jackman A, Heuckeroth RO, Snider WD, et al. (1998) GFR alpha1-deficient mice have deficits in the enteric nervous system and kidneys. Neuron 21: 317–324.
25. Karner CM, Chirumamilla R, Aoki S, Igarashi P, Wallingford JB, et al. (2009) Wnt9b signaling regulates planar cell polarity and kidney tubule morphogenesis. Nat Genet 41: 793–799.
26. Nishinakamura R, Matsumoto Y, Nakao K, Nakamura K, Sato A, et al. (2001) Murine homolog of SALL1 is essential for ureteric bud invasion in kidney development. Development 128: 3105–3115.
27. Quaggin SE, Kreidberg JA (2008) Development of the renal glomerulus: good neighbors and good fences. Development 135: 609–620.
28. Cubas R, Zhang S, Li M, Chen C, Yao Q (2010) Trop2 expression contributes to tumor pathogenesis by activating the ERK MAPK pathway. Mol Cancer 9: 253.
29. Adams JC, Watt FM (1993) Regulation of development and differentiation by the extracellular matrix. Development 117: 1183–1198.
30. Chen D, Roberts R, Pohl M, Nigam S, Kreidberg J, et al. (2004) Differential expression of collagen- and laminin-binding integrins mediates ureteric bud and inner medullary collecting duct cell tubulogenesis. Am J Physiol Renal Physiol 287: F602–611.
31. Korhonen M, Ylanne J, Laitinen L, Virtanen I (1990) The alpha 1-alpha 6 subunits of integrins are characteristically expressed in distinct segments of developing and adult human nephron. J Cell Biol 111: 1245–1254.
32. Hynes RO (2002) Integrins: bidirectional, allosteric signaling machines. Cell 110: 673–687.
33. Schwartz MA, Ginsberg MH (2002) Networks and crosstalk: integrin signalling spreads. Nat Cell Biol 4: E65–68.
34. Madin SH, Darby NB (1958) Established kidney cell lines of normal adult bovine and ovine origin. Proc Soc Exp Biol Med 98: 574–576.
35. Gardner H, Kreidberg J, Koteliansky V, Jaenisch R (1996) Deletion of integrin alpha 1 by homologous recombination permits normal murine development but gives rise to a specific deficit in cell adhesion. Dev Biol 175: 301–313.
36. Chen J, Diacovo TG, Grenache DG, Santoro SA, Zutter MM (2002) The alpha(2) integrin subunit-deficient mouse: a multifaceted phenotype including defects of branching morphogenesis and hemostasis. Am J Pathol 161: 337–344.
37. Saelman EU, Keely PJ, Santoro SA (1995) Loss of MDCK cell alpha 2 beta 1 integrin expression results in reduced cyst formation, failure of hepatocyte growth factor/scatter factor-induced branching morphogenesis, and increased apoptosis. J Cell Sci 108(Pt 11): 3531–3540.
38. Montesano R, Matsumoto K, Nakamura T, Orci L (1991) Identification of a fibroblast-derived epithelial morphogen as hepatocyte growth factor. Cell 67: 901–908.
39. Liu Y, Chattopadhyay N, Qin S, Szekeres C, Vasylyeva T, et al. (2009) Coordinate integrin and c-Met signaling regulate Wnt gene expression during epithelial morphogenesis. Development 136: 843–853.
40. Zhang Z, Pascuet E, Hueber PA, Chu L, Bichet DG, et al. (2010) Targeted inactivation of EGF receptor inhibits renal collecting duct development and function. J Am Soc Nephrol 21: 573–578.
41. Miyazaki Y, Oshima K, Fogo A, Hogan BL, Ichikawa I (2000) Bone morphogenetic protein 4 regulates the budding site and elongation of the mouse ureter. J Clin Invest 105: 863–873.
42. Mitra SK, Hanson DA, Schlaepfer DD (2005) Focal adhesion kinase: in command and control of cell motility. Nat Rev Mol Cell Biol 6: 56–68.
43. Balzar M, Bakker HA, Briaire-de-Bruijn IH, Fleuren GJ, Warnaar SO, et al. (1998) Cytoplasmic tail regulates the intercellular adhesion function of the epithelial cell adhesion molecule. Mol Cell Biol 18: 4833–4843.
44. Thesleff I, Vaahtokari A, Partanen AM (1995) Regulation of organogenesis. Common molecular mechanisms regulating the development of teeth and other organs. Int J Dev Biol 39: 35–50.
45. Lin Y, Zhang S, Tuukkanen J, Peltoketo H, Pihlajaniemi T, et al. (2003) Patterning parameters associated with the branching of the ureteric bud regulated by epithelial-mesenchymal interactions. Int J Dev Biol 47: 3–13.
46. Stefanini M, De Martino C, Zamboni L (1967) Fixation of ejaculated spermatozoa for electron microscopy. Nature 216: 173–174.
47. Morita S, Kojima T, Kitamura T (2000) Plat-E: an efficient and stable system for transient packaging of retroviruses. Gene Ther 7: 1063–1066.

メダカとゼブラフィッシュを用いた肝研究

浅岡洋一，仁科博史

大規模スクリーニングが可能な小型魚類メダカおよびゼブラフィッシュを用いて，これまでに多様な肝形成・肝機能不全変異体が単離されている．そのなかには既知のノックアウトマウスとは異なる表現型を示す興味深い変異体も数多く含まれる．変異体の単離から原因遺伝子の同定への流れがますます加速するなかで，小型魚類は肝形成のシグナル伝達ネットワークの分子基盤の解明ならびに創薬スクリーニングによる医薬品の開発に大いに貢献することが期待されている．

キーワード● 肝発生，肝疾患，メダカ，ゼブラフィッシュ

はじめに

近年の*in vitro*組織培養系の進歩や遺伝子破壊マウスの解析により，肝形成に関与するシグナルネットワークの実体は徐々に明らかになりつつあるが，母体内の子宮で発生するマウス胚を用いた肝臓発生研究にはさまざまな困難が伴う．例えば，①マウスは胎生であるため外部から生きたまま経時的に観察することが難しいこと，②突然変異体の大規模スクリーニングが困難であること，さらには③マウス胚では造血と肝形成が密接に関連しており，造血不全は致死あるいは二次的な肝形成異常を引き起こすことなどが挙げられる．そのため，母体外で発生し，小型で薬剤スクリーニングに適した新たなモデル生物が求められている．本稿では，器官発生・疾患モデル生物として脚光を浴びている小型魚類を用いた，肝形成および肝疾患に関する研究の現状を紹介する．

1 小型魚類を用いた肝形成研究

❶ 小型魚類モデルのメリットと注意点

モデル生物として確立されたゼブラフィッシュとメダカは，①卵生で胚が透明なため，肝形成過程を生きたまま経時的に観察できる（蛍光タンパク質を用いて細胞レベルでのライブイメージングが可能である），②細胞移植やトランスジェニック作製などの胚操作が比較的容易である，③モルフォリノアンチセンスオリゴを用いた遺伝子の機能阻害実験ができる，④ゲノムサイズが小さいことに加え，飼育スペースや経費が節約できるため，突然変異体の大規模スクリーニングが可能である，⑤体表からの受動的な酸素の拡散により，血液循環器系の障害による酸素不足を回避できる，さらに⑥初期造血が血島と腎臓で行われるため，発生中の肝臓に障害が生じても貧血症が生じないなど，マウス胚での研究上の問題点をクリアできる多くの特徴をもつ．一方，マウスではES細胞を用いた遺伝子破壊マウスの作出が容易になっているが，小型魚類では特定遺伝子の破壊実験はまだ一般的には普及していない．

Small fish as models for studying liver development and disease

Yoichi Asaoka/Hiroshi Nishina：Department of Developmental and Regenerative Biology, Medical Research Institute, Tokyo Medical and Dental University（東京医科歯科大学難治疾患研究所発生再生生物学分野）

表1　ゼブラフィッシュ肝形成・肝機能不全変異体

ゼブラフィッシュ変異体	遺伝子名	表現型	機能	文献
lumpazi	不明	肝臓のネクローシス	不明	4
gammier	不明	肝臓のネクローシス	不明	4
tramp	不明	肝臓のネクローシス	不明	4
tippelbruder	不明	肝臓における赤血球の蓄積	不明	4
beefeater	不明	肝臓の変性	不明	5
prometheus	*wnt2bb (wingless-type MMTV integration site family, member 2Bb)*	肝特異化の異常	canonical Wntシグナルを介した肝特異化制御	8
daedalus	*fgf10a (fibroblast growth factor 10a)*	肝特異化の異常	Fgfシグナルを介した肝特異化制御	7
lost-a-fin	*acvr1l (activin A receptor, type I like)*	肝特異化の異常	Bmpシグナルを介した肝特異化制御	9
hnf1ba	*hnf1ba (HNF1 homeobox Ba)*	肝特異化の異常	転写制御	25
uhrf1	*uhrf1 (ubiquitin-like, containing PHD and RING finger domains, 1)*	肝芽の成長不全	細胞周期制御・転写制御	26
ppp1r12a	*ppp1r12a (protein phosphatase 1, regulatory (inhibitor) subunit 12A)*	肝芽形成不全	ミオシン軽鎖の脱リン酸化	27
diexf	*diexf (digestive organ expansion factor homolog)*	肝臓低形成	p53シグナルを介した細胞周期制御	28
nil per os	*rbm19 (RNA binding motif protein 19)*	肝臓低形成	RNA結合	29
dandelion	*dnmt1 (DNA (cytosine-5-)-methyltransferase 1)*	肝臓低形成	DNAのメチル化	10
hdac1	*hdac1 (histone deacetylase 1)*	肝臓低形成	ヒストンの脱アセチル化	11

TILLING法[1]やZinc Finger Nuclease法[2]などの有望な遺伝子改変技術の普及により，遺伝子破壊ゼブラフィッシュ・メダカの作出が容易になると期待される．

❷ ゼブラフィッシュによる肝研究成果

ゼブラフィッシュのゲノムサイズ（1,700 Mb）はヒトやマウスの約半分であり，ゲノム情報やバイオリソースなど研究環境の整備が進んでいる．特に1990年代には，ドイツのチュービンゲンとアメリカのボストンにて大規模な変異体スクリーニングが行われ，数百に及ぶ変異体が単離された[3]．消化器系に異常を示すゼブラフィッシュ変異体も複数単離されており，そのうち肝形成に関与するものとしては，肝臓の細胞死を呈する*beefeater*など10種類以上が存在する（表1）[4][5]．また，Stainierらのグループは，すべての内胚葉でGFPが発現するトランスジェニック系統を樹立し，この系統を用いて肝臓の出芽形成や形態など詳細な観察と記述を報告しているほか，内胚葉形成異常の変異体スクリーニングを行っている[6]．2000年代後半になるとゼブラフィッシュ肝形成・肝機能不全変異体の原因遺伝子が次々と同定され，哺乳類同様にWnt，Fgf，およびBmpシグナル伝達経路が肝特異化に必須であることが明らかとなった[7]～[9]．さらに最近になって，ゼブラフィッシュ肝臓低形成変異体の解析が進み，DNAメチル化やヒストン脱アセチル化などのエピジェネティック修飾の異常と肝形成不全との関連が報告されており，新たな肝形成制御機構の可能性が示された[10][11]．

❸ メダカによる肝研究の利点と比較解析

一方，日本産のモデル生物であるメダカ（図1A）は，ゼブラフィッシュにはない以下の利点を兼ね備えている．すなわち①ゲノムサイズが800 Mb（ゼブラフィッシュの半分）であり，全ゲノム配列の解読プロジェクトがすでに完了していること[12]，②胚発生後期においても胚が透明で内臓器官を観察しやすいこと（図1B），③近交系が存在すること，さらに加えて④生育温度幅が広く（14～34℃）温度感受性変異体の単離も可能であることなどが挙げられる．このようなゲノム

A

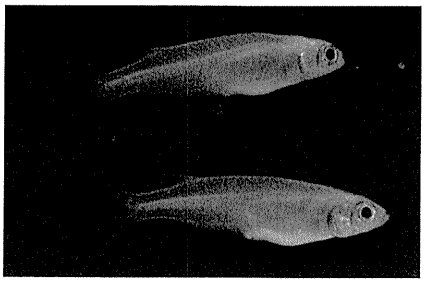

B

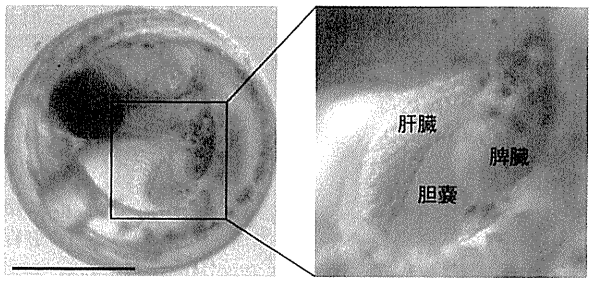

C

メダカグループ	変異体名	遺伝子名	表現型	文献
①肝芽形成不全	*hirame*	不明	中内胚葉の体軸への移行異常	14
	mochizuki	不明	*foxA3*発現消失	14
	akatsuki	不明	*foxA3*発現消失	14
	akebono	不明	*foxA3*発現消失	14
	fukuwarai	不明	肝芽の消失	14
	sakura	不明	肝芽の消失	14
②肝臓低形成	*hiohgi*	*raldh2*	肝臓サイズの減少	15
	kakurembo	不明	肝臓サイズの減少と前方への位置異常	14
	kamifusen	不明	肝臓に血液の蓄積	14
	origami	不明	肝臓形態異常	14
③肝臓位置異常	*kendama*	不明	肝臓と胆嚢の左右位置異常，脂肪肝	14
	dendendaiko	不明	肝臓と胆嚢の左右逆位	14
	hanetsuki	不明	肝臓と胆嚢の左右逆位	14
④胆嚢色異常	*akane*	不明	胆嚢が赤色	14
	suou	不明	胆嚢がオレンジ色	14
	ominaeshi	不明	胆嚢が無色	14
⑤脂質代謝異常	*ukon*	不明	PED6代謝不全	14
	aonibi	不明	PED6代謝不全	14
	uguisucha	不明	PED6代謝不全	14

図1　メダカを用いた大規模変異体スクリーニング

A）メダカ成魚．B）メダカ胚の肝臓・胆嚢・脾臓．メダカ胚は母体外で発生し，胚体が透明であるため，実体顕微鏡下で肝臓を含む内臓器官を生きたまま観察可能である．スケールバー＝500μm．C）肝形成・肝機能不全メダカ変異体リスト

サイズや形態の特徴から，ゼブラフィッシュでは得られないユニークな変異体の単離が期待され，1998～2003年にかけてメダカを用いた大規模スクリーニングが行われた（ERATO近藤誘導分化プロジェクト）[13]．われわれのグループもこのプロジェクトに参画し，肝形成や肝機能不全変異体を複数単離することに成功した[14]．得られた19種の変異体は，その表現型から5つのグループ（第1群：肝芽形成不全，第2群：肝臓低形成，第3群：肝臓位置異常，第4群：胆嚢色異常，第5群：脂質代謝異常）に分類された（図1C）．

このうち第2群に属する*hiohgi*変異体は，肝臓が小さいうえに胸鰭がないという興味深い表現型を示す．原因遺伝子の同定により，*hiohgi*変異はビタミンAからオールトランスレチノイン酸（RA）を合成する酵素（レチノイン酸合成酵素タイプ2，RALDH2）をコードする遺伝子の変異であることが判明した．詳細な解析から，体節に発現するRALDH2がRAを産生し，産生されたRAが下流に位置する*wnt2bb*遺伝子の発現を側板中胚葉に誘導することにより，肝臓の特異化が決定されることが示された（図2A）．ゼブラフィッシュ*wnt2bb*変異体（*prometheus*）においても肝特異化の異常とそれに伴う肝臓発生の遅延が認められており，

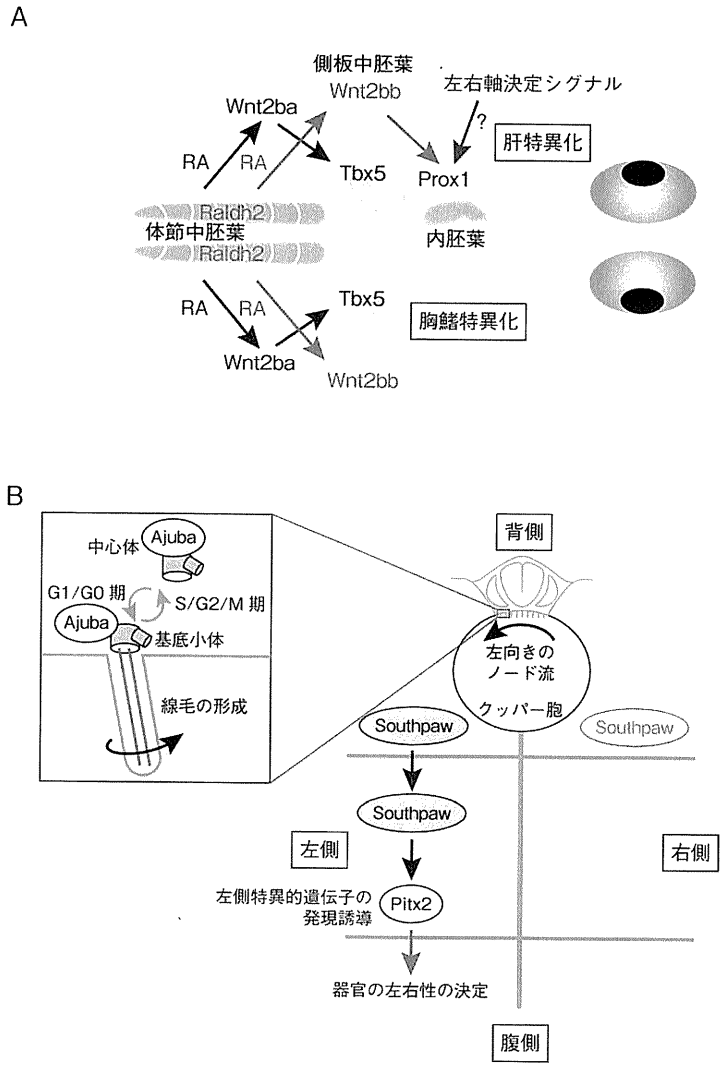

図2　メダカの肝特異化機構と左右軸決定機構

A）メダカの肝特異化と胸鰭特異化を制御するシグナル伝達系．メダカ肝特異化ならびに胸鰭特異化のシグナル伝達系は類似している．B）Ajubaによる器官の左右性の決定機構

さらに*wnt2*を同時に機能阻害すると肝臓は全く発生しない（Oberら FASEB meeting 2010にて発表）．このことは*wnt2*と*wnt2bb*の両者が肝特異化とその後の肝形成に必須の役割を果たしていることを示唆する．興味深いことに，RALDH2による*wnt*遺伝子誘導のシグナル系は，胸鰭の特異化を決定するシグナル系と酷似している（図2 A）．マウス前脚およびゼブラフィッシュ胸鰭の形成にはRALDH2が必須の役割を果たし，その下流にWntやTbxのシグナル分子が存在することはこれまでに報告されてきた．しかしながら，RALDH2ノックアウトマウスやゼブラフィッシュ変異体は肝形成以前に致死または広範囲にわたるパターニングの異常を伴うことから，肝形成におけるRALDH2の役割については未解明であった．*hiohgi*メダカ変異体の解析によってはじめてRALDH2の肝特異化における役割が明らかとなったことは，ゼブラフィッシュ変異体とメダカ変異体の比較解析の重要性を改めて示したと言えよう[15]．

表2　肝疾患モデルとしてのメダカとゼブラフィッシュ

肝疾患	疾患モデル動物	文献
肝癌	DENA誘発肝腫瘍メダカ	20
	MAMアセテート誘発肝腫瘍メダカ	19
	自然発生肝腫瘍メダカ	21
	DMBAまたはDBP誘発肝腫瘍ゼブラフィッシュ	30
脂肪肝	γ-hexachlorocyclohexane誘発脂肪肝ゼブラフィッシュ	31
	TAA誘発脂肪肝ゼブラフィッシュ	32
	アルコール誘発脂肪肝ゼブラフィッシュ	33
	*foie gras*ゼブラフィッシュ変異体	22
	*ducttrip*ゼブラフィッシュ変異体	34
肝腫大	*nf2*ゼブラフィッシュ変異体	22
	*vps18*ゼブラフィッシュ変異体	22
NASH	高脂肪食誘発NASH様メダカ	23，24

❹ 線毛形成と左右軸決定シグナルの制御

肝臓が体軸の正しい位置に形成され正常な機能を発揮するためには，左右軸決定シグナルによる制御が不可欠である（図2A）．われわれは肝形成に関与する左右軸決定シグナルの解析過程において，LIMタンパク質Ajubaのメダカ機能阻害胚が興味深い表現型を示すことを見出した．すなわちAjubaの発現抑制により，肝臓を含む内臓器官の左右位置異常が生じること，左側特異的シグナル分子が異所性発現を示すこと，左右性を生み出すクッパー上皮細胞の線毛が短縮することを明らかにした．これまでAjubàは分裂期の中心体において紡錘体形成に関与することが報告されていたが，前述の解析によりAjubaが間期の基底小体における線毛形成の制御を介して器官の左右性決定に関与することが示唆された（図2B）[16]．

2 小型魚類を用いた肝疾患モデルの作出

小型魚類はヒト疾患モデルとして医学分野における貢献度も増している．例えば，メダカのパーキンソン病モデルは神経変性疾患の病態生理解析の有用なモデル系となっている[17]．また，小型魚類は毒物標的探索モデルとしても利用価値が高く，サリドマイド催奇性機構の解明などに大いに貢献している[18]．一方，肝疾患モデルとしては日本では古くからメダカを用いた腫瘍誘発研究が行われており，メダカは肝腫瘍モデルとして肝発癌分子機構の解明に寄与してきた（表2）[19)～21]．さらに近年では，脂肪性肝疾患のモデル生物として小型魚類が注目を集めており，Sadlerらは変異体スクリーニングによって脂肪肝ゼブラフィッシュ“*foie gras*（フォアグラ）”を単離している[22]．われわれもメダカ変異体の再スクリーニングにより，“*kendama*”変異体が生後60～80日において脂肪肝を発症することを見出している（図1C）．また，山口大学のグループは，高脂肪食をメダカに摂取させることによって非アルコール性脂肪性肝炎（NASH）を発症させることにも成功しており，ヒトと類似の病理所見や遺伝子発現の変化が観察された[23) 24]．このメダカNASHモデルに各種薬剤を投与することにより，NASHに改善が認められるかどうかの評価スクリーニングを行ったところ，興味深いことに，多価不飽和脂肪酸であるEPAの同時投与によってNASHの発症は抑制された．欧米ではすでにゼブラフィッシュを用いたハイスループット薬剤スクリーニングが行われている．マウスに比較してスクリーニングできる薬剤の数は百倍以上，繁殖や飼育にかかる実験費用も数十分の1以下という利点があり，そのため，ヒト疾患を模倣する変異体の単離が注目されている．脂肪肝を前段階として，線維化，NASH，肝硬変へ進行する症例や，肝硬変を経て肝癌を発症する症例も報告されており，重篤な肝疾患を予防する方法の1つとして，脂肪肝を軽減させることが有効と考えられる．*kendama*メダカ変異体や高脂肪食摂取によるNASH様メダカを用いた脂肪肝発症機構の解明と創薬研究が期待されている．

おわりに

本稿では小型魚類を用いた肝発生ならびに肝疾患研究の現状を中心に紹介してきた．誌面の都合で触れることができなかったが，小型魚類は肝再生研究の分野においてもその特徴を活かした研究が進展しており，再生実験モデル生物としての地位も確立しつつある．脊椎動物の肝臓発生・再生システムの全体像を理解するうえで，今後も優れたモデル生物として小型魚類の果たす役割はきわめて大きいと考えている．

謝辞

メダカ変異体のスクリーニングは，現 英国バース大学再生医学センターの古谷-清木誠博士，大阪大学 近藤寿人教授のご指導のもと行われました．お世話になった先生方にこの場を借りて感謝致します．

文献

1) Moens, C. B. et al. : Brief. Funct. Genomic. Proteomic., 7 : 454-459, 2008
2) Doyon, Y. et al. : Nat. Biotechnol., 26 : 702-708, 2008
3) Zebrafish Special Issue : Development, 123 : 1-461, 1996
4) Chen, J. N. et al. : Development, 123 : 293-302, 1996
5) Pack, M. et al. : Development, 123 : 321-328, 1996
6) Field, H. A. et al. : Dev. Biol., 253 : 279-290, 2003
7) Dong, P. D. et al. : Nat. Genet., 39 : 397-402, 2007
8) Ober, E. A. et al. : Nature, 442 : 688-691, 2006
9) Shin, D. et al. : Development, 134 : 2041-2050, 2007
10) Anderson, R. M. et al. : Dev. Biol., 334 : 213-223, 2009
11) Noel, E. S. et al. : Dev. Biol., 322 : 237-250, 2008
12) Kasahara, M. et al. : Nature, 447 : 714-719, 2007
13) Medaka Special Issue : Mech. Dev., 121 : 593-1008, 2004
14) Watanabe, T. et al. : Mech. Dev., 121 : 791-802, 2004
15) Negishi, T. et al. : Hepatology, 51 : 1037-1045, 2010
16) Nagai, Y. et al. : Biochem. Biophys. Res. Commun., 396 : 887-893, 2010
17) Matsui, H. et al. : J. Neurochem., 115 : 178-187, 2010
18) Ito, T. et al. : Science, 327 : 1345-1350, 2010
19) Aoki, K. & Matsudaira H. : J. Natl. Cancer Inst., 59 : 1747-1749, 1977
20) Ishikawa, T. et al. : J. Natl. Cancer Inst., 55 : 909-916, 1975
21) Masahito, P. et al. : Jpn. J. Cancer Res., 80 : 1058-1065, 1989
22) Sadler, K. C. et al. : Development, 132 : 3561-3572, 2005
23) Kuwashiro, S. et al. : Cell Tissue Res., 344 : 125-134, 2011
24) Matsumoto, T. et al. : Dis. Model. Mech., 3 : 431-440, 2010
25) Lokmane, L. et al. : Development, 135 : 2777-2786, 2008
26) Sadler, K. C. et al. : Proc. Natl. Acad. Sci. USA, 104 : 1570-1575, 2007
27) Huang, H. et al. : Development, 135 : 3209-3218, 2008
28) Chen, J. et al. : Genes Dev., 19 : 2900-2911, 2005
29) Mayer, A. N. & Fishman, M. C. : Development, 130 : 3917-3928, 2003
30) Lam, S. H. et al. : Nat. Biotechnol., 24 : 73-75, 2006
31) Braunbeck, T. et al. : Ecotoxicol. Environ. Saf., 19 : 355-374, 1990
32) Amali, A. A. et al. : J. Biomed. Sci., 13 : 225-232, 2006
33) Passeri, M. J. et al. : Hepatology, 49 : 443-452, 2009
34) Matthews, R. P. et al. : Development, 136 : 865-875, 2009

Profile 筆頭著者プロフィール

浅岡洋一：2000年，東京大学理学部生物化学科卒業．'06年，同大学院理学系研究科生物化学専攻博士課程修了，理学博士．日本学術振興会特別研究員を経て，同年より東京医科歯科大学難治疾患研究所発生再生生物学分野助教，現在に至る．研究テーマ：ゼブラフィッシュを用いたストレス応答性シグナル伝達系に関する研究，およびメダカ突然変異体を用いた初期胚の器官形成に関する研究．

Biochemical and Biophysical Research Communications 408 (2011) 120–125

Contents lists available at ScienceDirect

Biochemical and Biophysical Research Communications

journal homepage: www.elsevier.com/locate/ybbrc

Imaging mass spectrometry reveals characteristic changes in triglyceride and phospholipid species in regenerating mouse liver

Norio Miyamura [a,1], Takashi Nakamura [a,1], Naoko Goto-Inoue [b], Nobuhiro Zaima [b], Takahiro Hayasaka [b], Tokiwa Yamasaki [a], Shuji Terai [c], Isao Sakaida [c], Mitsutoshi Setou [b], Hiroshi Nishina [a,*]

[a] Dept. Developmental and Regenerative Biology, Medical Research Institute, Tokyo Medical and Dental University, Tokyo, Japan
[b] Dept. Molecular Anatomy, Hamamatsu University School of Medicine, Shizuoka, Japan
[c] Dept. Gastroenterology and Hepatology, Yamaguchi University Graduate School of Medicine, Yamaguchi, Japan

ARTICLE INFO

Article history:
Received 25 March 2011
Available online 2 April 2011

Keywords:
Imaging mass spectrometry
Metabolite imaging
Liver regeneration
MALDI-TOF

ABSTRACT

After partial hepatectomy (PH), regenerating liver accumulates unknown lipid species. Here, we analyzed lipids in murine liver and adipose tissues following PH by thin-layer chromatography (TLC), imaging mass spectrometry (IMS), and real-time RT-PCR. In liver, IMS revealed that a single TLC band comprised major 19 TG species. Similarly, IMS showed a single phospholipid TLC band to be major 13 species. In adipose tissues, PH induced changes to expression of genes regulating lipid metabolism. Finally, IMS of phosphatidylcholine species demonstrated distribution gradients in lobules that resembled hepatic zonation. IMS is thus a novel and power tool for analyzing lipid species with high resolution.

1. Introduction

The liver has a remarkable capacity to regenerate after injury [1,2] and partial hepatectomy (PH) in rodents has been useful for investigating the underlying mechanisms. Following PH, hepatocytes in the remaining liver tissue start proliferating such that normal liver mass is restored; the regenerative response is then terminated. To support this hepatocyte proliferation, the liver remnant transiently accumulates lipids that supply the energy and membrane components needed for cell division [3–5]. However, it is unclear what molecular species of lipids are involved and whether PH affects other tissues.

Matrix-assisted laser desorptional/ionization (MALDI) mass spectrometry is often used to analyze low molecular weight compounds such as lipids. A recent refinement called "imaging mass spectrometry" (IMS) allows visualization of the amount and distribution of individual molecular species in tissue sections [6,7]. IMS has successfully revealed changes in lipid identity, amount and distribution in tissue sections of plants and animals [8–11]. In this study, we used IMS to identify lipid species in murine liver regenerating after PH. We also carried out gene expression analysis to define the effects of PH on adipose tissues, which are important for lipid metabolism.

2. Materials and methods

2.1. Reagents

All chemicals used were of the highest purity, including trifluoroacetic acid (TFA) and methanol (Kanto Chemical, Japan) and 2,5-dihydroxybenzoic acid (DHB) (Bruker Daltonics, Germany). Ultrapure water from a Milli-Q system (Millipore, USA) was used for all buffers and solvents.

2.2. Animals

Female C57BL/6J mice (10 weeks old; CLEA Japan Inc.) were kept in a temperature-controlled room with a 12 h dark/light cycle and fed CE-2 diet (CLEA). PH or sham surgery was performed as described [12] between 9 and 10 a.m. and animals were sacrificed at 0, 6, 12 or 24 h post-operation. All animal experiments were conducted according to the guidelines of Tokyo Medical and Dental University.

Abbreviations: BAT, brown adipose tissue; CE, cholesterol ester; Chol, cholesterol; DG, diacylglycerol; FA, fatty acid; FFA, free fatty acids; IMS, imaging mass spectrometry; LPC, lysophosphatidylcholine; MALDI-TOF, matrix-assisted laser desorptional ionization-time of flight; PC, phosphatidylcholine; PE, phosphatidylethanolamine; PH, partial hepatectomy; PI, phosphatidylinositol; PS, phosphatidylserine; SM, sphingomyelin; SCF, subcutaneous fat; TG, triglyceride; VF, visceral fat.

* Corresponding author. Address: 1-5-45 Yushima, Bunkyo-ku, Tokyo 113-8510, Japan. Fax: +81 3 5803 5829.
E-mail address: nishina.dbio@mri.tmd.ac.jp (H. Nishina).

[1] These authors contributed equally to this work as first authors.

0006-291X/$ - see front matter © 2011 Elsevier Inc. All rights reserved.
doi:10.1016/j.bbrc.2011.03.133

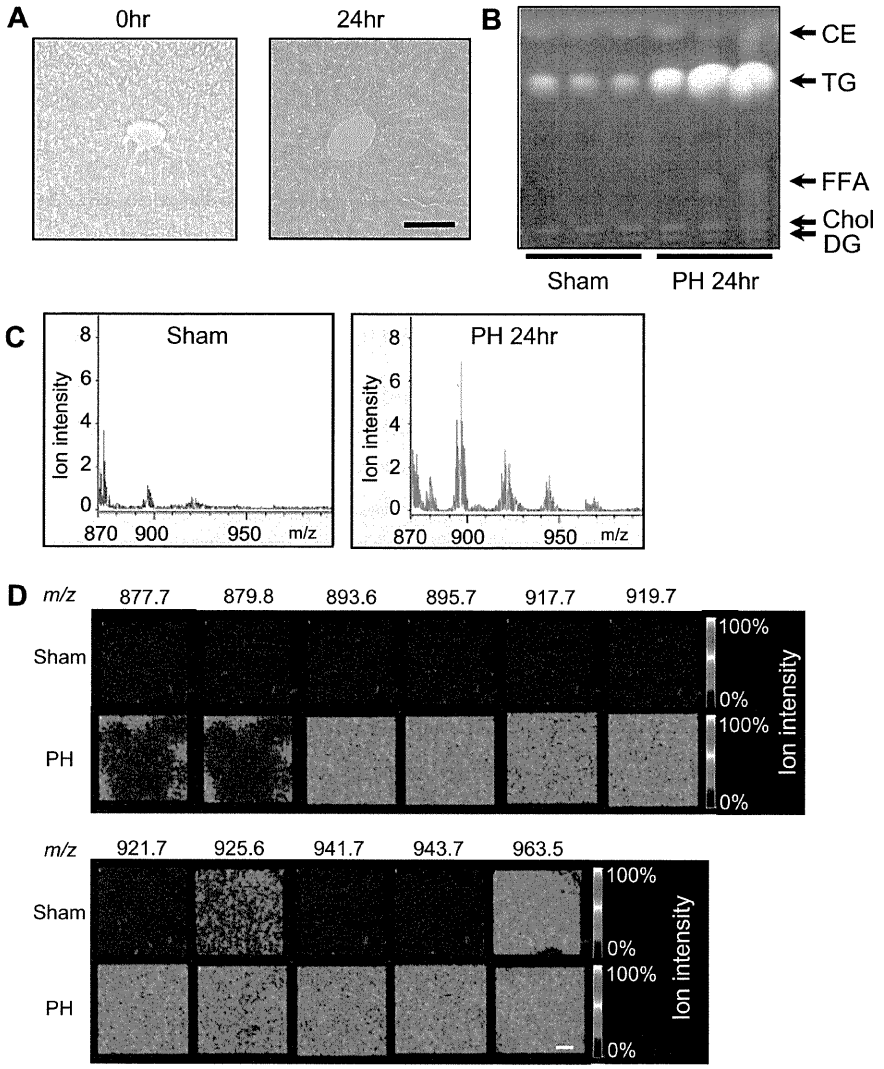

Fig. 1. Dramatic changes of multiple triglyceride species in concentration during liver regeneration. (A) Oil red O-stained liver sections showing increased TG (red) globules in hepatocytes at 24 h post-PH. Scale bar, 100 μm. (B) TLC of neutral lipids in liver extracts from mice at 24 h post-PH or sham surgery. For all experiments, results shown are representative of 3 mice/group. (C) MALDI-TOF average mass spectra of liver from mice at 24 h post-PH or sham surgery. A range from 875 *m/z* to 1000 was examined. (D) MALDI-TOF-MS imaging of lipid ion species in liver sections from the mice in (C). Scale bar, 500 μm.

2.3. Oil red O staining

Frozen liver sections were prepared using O.C.T Compound (Sakura Finetek, Japan) and a cryostat (CM 1950; Leica Microsystems, Germany) set to 10 μm. Oil red O staining was performed as described [13].

2.4. Lipid extraction and thin-layer chromatography

Liver lipids were extracted using chloroform:methanol (2:1) as described [14]. For TLC, Silica Gel 60 plates (Merck, USA) were run in n-hexane:diethyl ether:acetic acid (80:30:1) to separate neutral lipids, and in methyl acetate:propanol:chloroform:methanol:0.2% KCl (25:25:25:10:9) to resolve phospholipids. Lipids were visualized using primuline (Nakarai Tesque, Japan) and identified based on migration compared to standards [15].

2.5. Quantitative real-time RT-PCR

Quantitative real-time RT-PCR was performed as described [16]. Primer sequences are listed in Supplementary Information (Table S1).

2.6. IMS samples

IMS samples were prepared as previously described [10,17] with a slight modification. Frozen liver cryostat sections (8 μm) were mounted on indium-tin-oxide-coated glass slides (Bruker Daltonics). DHB matrix solution (50 mg/ml DHB in 70% methanol/0.1% TFA) was sprayed uniformly over mounted sections with a 0.2 mm nozzle airbrush (Mr. Hobby, Japan).

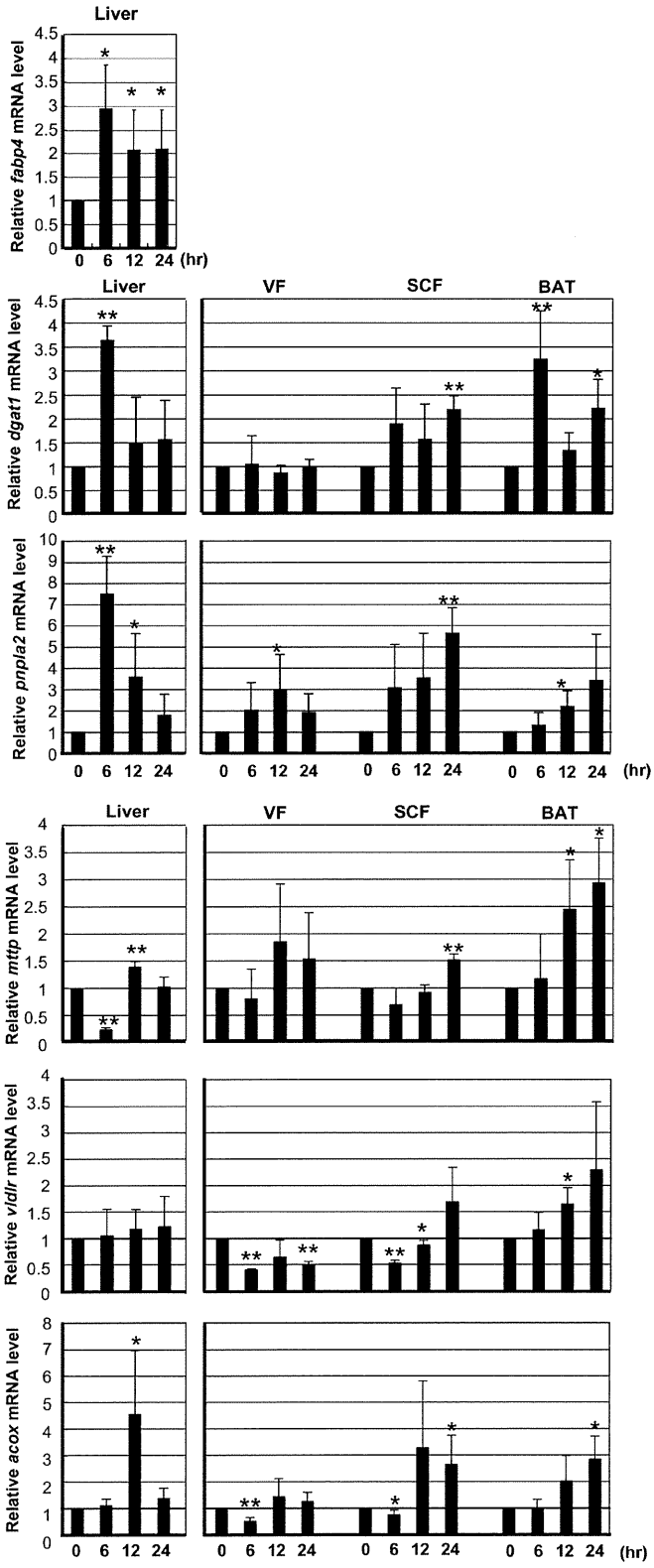

Fig. 2. mRNA levels of the indicated TG metabolism-related and β-oxidation-related genes in liver, visceral fat, subcutaneous fat and BAT. Data are mean fold induction ± SD relative to *gapdh*. $n = 3$ $^{*}p < 0.05$, $^{**}p < 0.01$ vs. value at 0 h.

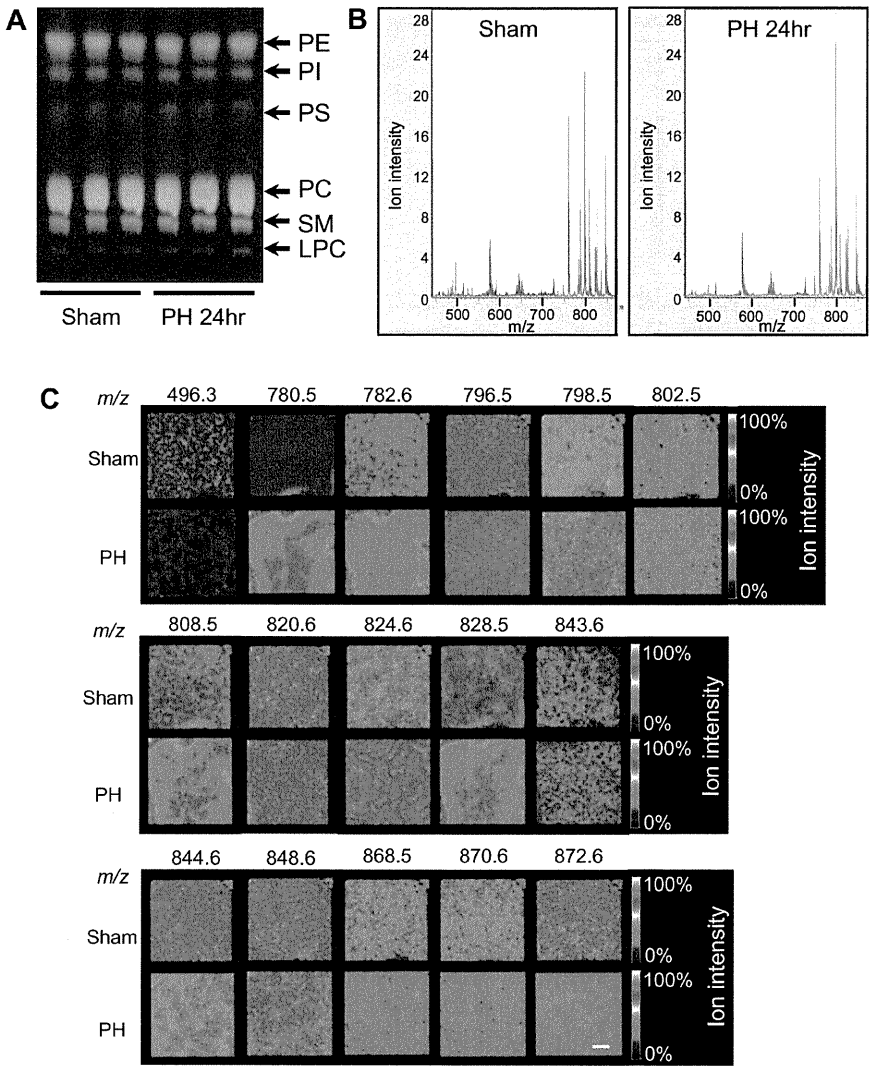

Fig. 3. The existence and dynamic distribution of clearly multiple phospholipids. (A) TLC of phospholipids in liver extracts from mice at 24 h post-PH or sham surgery. (B) MALDI-TOF mass spectra of liver extracts from mice at 24 h post-PH or sham surgery. A range from 440 *m/z* to 875 was examined. (C) MALDI-TOF-MS imaging of lipid ion species in liver sections from the mice in (B). Scale bar, 500 μm.

2.7. MALDI-TOF IMS

MALDI mass spectrometry was performed using an Ultraflex II TOF/TOF instrument (Bruker Daltonics) equipped with a 355 nm Nd:YAG laser with a 200 Hz repetition rate. The measurement pitch was 50 μm. Data were acquired in positive-ion mode using an external calibration method. Mass spectrometer parameters were set to obtain *m/z* values of 400–2000. All spectra were acquired automatically with FlexImaging software (Bruker Daltonics). The laser was irradiated 200 times per position. Peaks were normalized to total ion current and compared. The Lipid Search (http://lipid-search.jp) database were used to determine lipid molecular species.

3. Results

3.1. Multiple triglyceride species in regenerating liver

Oil red O staining of hepatocytes in regenerating liver at 24 h post-PH revealed an accumulation of TG that did not appear in sham-treated livers (Fig. 1A). TLC of extracted total lipids from these livers revealed bands of CE, TG, FFA, Chol and DG that were increased or unchanged in extracts from PH livers (Fig. 1B). IMS analysis of liver sections at 24 h after sham treatment or PH revealed increases in PH livers of several peaks in the mass range from *m/z* 875 to *m/z* 1000 (Fig. 1C), 19 of which represented abundant TG molecular species (Table S2). The visualization of these data shown in Fig. 1D confirms that multiple TG species undergo dramatic changes in concentration during liver regeneration.

3.2. Changes to expression of lipid-related genes in regenerating liver and adipose tissues

Because adipose tissues are vital for lipid metabolism, we investigated whether PH affected these tissues as well as the liver. We examined gene expression patterns in liver, visceral fat (VF), subcutaneous fat (SCF) and brown adipose tissue (BAT) of animals subjected to PH or sham surgery. Specifically, we monitored the expression of *fabp4*, which encodes FFA binding protein and served

as a positive control; *dgat*, encoding an enzyme catalyzing the final stage of TG synthesis; *pnpla2*, encoding an enzyme catalyzing the first step in TG hydrolysis; *mttp*, encoding a protein involved in β-lipoprotein production; *vldlr*, important for the metabolism of apoprotein-E-containing TG-rich lipoproteins; and *acox*, encoding the first enzyme of the FA β-oxidation pathway. The mRNA levels of these genes as determined by real-time RT-PCR were normalized to the internal controls *gapdh* (Fig. 2) and *tubb2b* (data not shown), yielding similar results. Consistent with a previous report [18], *fabp4* was upregulated in regenerating liver, showing its highest induction at 6 h post-PH. The same pattern held true for upregulation of *dgat* and *pnpla2*, with *acox* peaking at 12 h post-PH. In contrast, *mttp* was downregulated at 6 h post-PH but upregulated over control levels by 12 h post-PH. The level of liver *vldlr* mRNA was not altered by PH. For *dgat1*, *pnpla2* and *acox*, mRNA levels had returned to baseline by 24 h post-PH. Interestingly, different expression patterns were observed in adipose tissues. At 6 h post-PH, *dgat1* mRNA was upregulated only in BAT whereas *pnpla2* tended to be upregulated only after 12 h post-PH. Unlike its pattern in liver, *mttp* mRNA was not downregulated in adipose tissues and steadily rose after 12 h post-PH. Levels of *vldlr*, which were unchanged in liver, were downregulated in VF. *Acox* mRNA was upregulated over control levels in SCF and BAT by 24 h post-PH. These results indicate that PH induces striking changes to lipid-related gene expression patterns in adipose tissues.

3.3. Phospholipids in regenerating liver

Phospholipids are a major component of all cell membranes and are important for liver regeneration. TLC of liver extracts from our PH- or sham-treated mice revealed equivalent bands of PE, PI, PS, PC, SM and LPC (Fig. 3A). IMS performed at 24 h post-PH or sham surgery showed several peaks in the mass range from *m/z* 440 to *m/z* 875 that were present in both PH liver and sham-treated liver (Fig. 3B). Of these, 11 were assigned by their masses to abundant PC molecular species, one to LPC and one to sphingomyelin (Table 1). Compared to sham-treated liver, levels of six putative PC species such as PC (1-acyl 34:2) and PC (1-acyl 36:5) and one sphingomyelin were increased in regenerating liver, whereas one putative LPC and two putative PC species were decreased. The IMS visualization of these molecular species shown in Fig. 3C clearly demonstrates the differences in levels of liver phospholipid species between PH- and sham-treated mice. In particular, the perivenous area of the sham-treated liver displayed lower levels of *m/z* 848.6 but higher levels of *m/z* 796.5 compared to periportal area. These results show that levels of phospholipid species change dynamically following PH, and that several of these species show a gradient in their intralobular distribution that is reminiscent of hepatic zonation [19].

Table 1
Changes to phospholipid species in post-PH liver sections as determined by MALDI-TOF-MS.

m/z	Change*	Putative molecular species
496.3	↓	LPC(16:0)
780.5	↑	PC(1-acyl 34:2) + Na
782.6	↑	PC(1-acyl 34:1) + Na
796.5	↑	PC(1-acyl 34:2) + K
798.5	↑	PC(1-acyl 34:1) + K
802.5	↑	PC(1-acyl 36:5)
808.5	↑	PC(1-acyl 36:2) + Na
820.6	→	PC(1-acyl 36:4)
824.6	↑	PC(1-acyl 36:2) + K
828.5	↑	PC(1-acyl 36:0)
843.6	↑	SM(2-amido22:2)
844.6	↑	PC(1-acyl 38:6)
848.6	→	PC(1-acyl 38:4)
868.5	↓	PC(1-acyl 40:8)
870.6	→	PC(1-acyl 40:7)
872.6	↓	PC(1-acyl 40:6)

↑, increase; ↓, decrease; →, unchanged; SM, sphingomyelin.
* Change relative to sham surgery.

4. Discussion

In this study, we have demonstrated that IMS can uncover previously hidden lipid species in regenerating liver after PH. We have also shown that PH not only affects liver lipids but also the expression of lipid-related genes in adipose tissues. The most common method used to analyze lipids in post-PH liver is TLC, which in our hands detected only a single band of TG that increased with time, as well as a collection of single phospholipid bands that did not change in intensity (Figs. 1B and 3A). In contrast, IMS revealed the existence and dynamic distribution of clearly multiple TGs (Fig. 1C and D, Table S2) and phospholipids (Fig. 3B and C, Table 1). Our results therefore demonstrate that IMS is a highly useful tool for both analyzing lipid species with high resolution.

Our results also show that PH affects the expression of genes that regulate TG synthesis, degradation and β-oxidation in adipose tissues (Fig. 2). Although adipose tissues are not directly connected to liver, they synthesize and release TGs that can travel in the blood to this organ. We propose that the injured liver may send an unidentified signal to the adipose tissues that regulates lipid metabolism. One possible route for such a signal might be via the blood. Indeed, it was recently reported that the serum total TG concentration was decreased by 75% at 6 h post-PH in mice [18]. The altered gene expression we observed in adipose tissues post-PH could result from cellular sensing of a reduction in blood TG. Another possibility may be signal transmission via the central nervous system (CNS). Imai et al. recently reported that hepatic ERK activation regulates pancreatic beta cell mass via the CNS [20]. Thus, following PH, hepatocytes may transmit a neural signal to adipose tissues that communicates their need to acquire more lipids for regeneration. Because the liver is a central metabolic regulator, interactions between the liver and other tissues mediated through the blood and/or CNS may be essential for whole body homeostasis.

Moreover, IMS allowed the 2D-visualization of TG and phospholipid distribution patterns in liver (Figs. 1D and 3C). Hepatic zonation refers to a gradient of molecules that appears from the perivenous region of a liver lobule to its periportal region [19]. We found that the perivenous area of the sham-treated liver displayed lower levels of *m/z* 848.6 but higher levels of *m/z* 796.5 compared to periportal area (Fig. 3C), consistent with hepatic zonation. Although a few previous studies have provided evidence of differential distribution of some mRNAs and proteins in liver lobules as determined by *in situ* hybridization and immunostaining, our IMS analysis is the first to show that small molecules such as lipids also exhibit hepatic zonation.

Increased fat content (steatosis) is a common feature of a liver under stress, be it due to regeneration after PH, or to altered function due to severe fasting. Prior to our study, it was not clear whether these fatty livers differed in their lipid content. Zaima et al. and van Ginneken et al. reported that PC (1-acyl 34:2) was the dominant lipid species increasing in the pathologic fatty liver induced in fasting mouse and rat models [21,22]. These groups therefore proposed that PC (1-acyl 34:2) is important for the evolution of fatty liver in this context. In our study, we too observed an increase in PC (1-acyl 34:2) in regenerating liver post-PH (Table 1). However, we also detected elevations in additional lipid species such as PC (1-acyl 36:5), which was decreased in fasting liver

[21,22]. PC (1-acyl 36:5) may therefore be a biomarker specific for steatosis induced by PH. Thus, MS and IMS are powerful tools that can assist in the detailed measurement of lipid metabolism.

Acknowledgments

This work was supported in part by research grants from the Ministry of Education, Culture, Sports, Science and Technology of Japan, the Ministry of Health, Labour and Welfare of Japan, and the Japan Society for the Promotion of Science.

Appendix A. Supplementary data

Supplementary data associated with this article can be found, in the online version, at doi:10.1016/j.bbrc.2011.03.133.

References

[1] G.K. Michalopoulos, M.C. DeFrances, Liver regeneration, Science 276 (1997) 60–66.
[2] S. Hata, M. Namae, H. Nishina, Liver development and regeneration: from laboratory study to clinical therapy, Development Growth and Differentiation 49 (2007) 163–170.
[3] T.J. Delahunt, D. Rubinste, Accumulation and release of triglycerides by rat liver following partial hepatectomy, Journal of Lipid Research 11 (1970) 536.
[4] A.B. Murray, W. Strecker, S. Silz, Ultrastructural-changes in rat hepatocytes after partial-hepatectomy, and comparison with biochemical results, Journal of Cell Science 50 (1981) 433–448.
[5] E.A. Glende, W.S. Morgan, Alteration in liver lipid and lipid fatty acid composition after partial hepatectomy in rat, Experimental and Molecular Pathology 8 (1968) 190.
[6] M. Stoeckli, P. Chaurand, D.E. Hallahan, R.M. Caprioli, Imaging mass spectrometry: a new technology for the analysis of protein expression in mammalian tissues, Nature Medicine 7 (2001) 493–496.
[7] M. Stoeckli, T.B. Farmer, R.M. Caprioli, Automated mass spectrometry imaging with a matrix-assisted laser desorption ionization time-of-flight instrument, Journal of the American Society for Mass Spectrometry 10 (1999) 67–71.
[8] T. Harada, A. Yuba-Kubo, Y. Sugiura, N. Zaima, T. Hayasaka, N. Goto-Inoue, M. Wakui, M. Suematsu, K. Takeshita, K. Ogawa, Y. Yoshida, M. Setou, Visualization of volatile substances in different organelles with an atmospheric-pressure mass microscope, Analytical Chemistry 81 (2009) 9153–9157.
[9] S. Shimma, Y. Sugiura, T. Hayasaka, N. Zaima, M. Matsumoto, M. Setou, Mass imaging and identification of biomolecules with MALDI-QIT-TOF-based system, Analytical Chemistry 80 (2008) 878–885.
[10] N. Goto-Inoue, T. Hayasaka, Y. Sugiura, T. Taki, Y.T. Li, M. Matsumoto, M. Setou, High-sensitivity analysis of glycosphingolipids by matrix-assisted laser desorption/ionization quadrupole ion trap time-of-flight imaging mass spectrometry on transfer membranes, Journal of Chromatography B-Analytical Technologies in the Biomedical and Life Sciences 870 (2008) 74–83.
[11] N. Zaima, T. Hayasaka, N. Goto-Inoue, M. Setou, Imaging of metabolites by MALDI mass spectrometry, Journal of Oleo Science 58 (2009) 415–419.
[12] C. Mitchell, H. Willenbring, A reproducible and well-tolerated method for 2/3 partial hepatectomy in mice, Nature Protocols 3 (2008) 1167–1170.
[13] E. Shteyer, Y.J. Liao, L.J. Muglia, P.W. Hruz, D.A. Rudnick, Disruption of hepatic adipogenesis is associated with impaired liver regeneration in mice, Hepatology 40 (2004) 1322–1332.
[14] J. Folch, M. Lees, G.H.S. Stanley, A simple method for the isolation and purification of total lipides from animal tissues, Journal of Biological Chemistry 226 (1957) 497–509.
[15] N. Goto-Inoue, T. Hayasaka, T. Taki, T.V. Gonzalez, M. Setou, A new lipidomics approach by thin-layer chromatography-blot-matrix-assisted laser desorption/ionization imaging mass spectrometry for analyzing detailed patterns of phospholipid molecular species, Journal of Chromatography A 1216 (2009) 7096–7101.
[16] J. Seo, Y. Asaoka, Y. Nagai, J. Hirayama, T. Yamasaki, M. Namae, S. Ohata, N. Shimizu, T. Negishi, D. Kitagawa, H. Kondoh, M. Furutani-Seiki, J.M. Penninger, T. Katada, H. Nishina, Negative regulation of wnt11 expression by Jnk signaling during zebrafish gastrulation, Journal of Cellular Biochemistry 110 (2010) 1022–1037.
[17] S. Taira, Y. Sugiura, S. Moritake, S. Shimma, Y. Ichiyanagi, M. Setou, Nanoparticle-assisted laser desorption/ionization based mass imaging with cellular resolution, Analytical Chemistry 80 (2008) 4761–4766.
[18] E.P. Newberry, S.M. Kennedy, Y. Xie, J. Luo, S.E. Stanley, C.F. Semenkovich, R.M. Crooke, M.J. Graham, N.O. Davidson, Altered hepatic triglyceride content after partial hepatectomy without impaired liver regeneration in multiple murine genetic models, Hepatology 48 (2008) 1097–1105.
[19] K. Jungermann, Zonation of metabolism and gene expression in liver, Histochemistry and Cell Biology 103 (1995) 81–91.
[20] J. Imai, H. Katagiri, T. Yamada, Y. Ishigaki, T. Suzuki, H. Kudo, K. Uno, Y. Hasegawa, J.H. Gao, K. Kaneko, H. Ishihara, A. Niijima, M. Nakazato, T. Asano, Y. Minokoshi, Y. Oka, Regulation of pancreatic beta cell mass by neuronal signals from the liver, Science 322 (2008) 1250–1254.
[21] N. Zaima, Y. Matsuyama, M. Setou, Principal component analysis of direct matrix-assisted laser desorption/ionization mass spectrometric data related to metabolites of fatty liver, Journal of Oleo Science 58 (2009) 267–273.
[22] V. van Ginneken, E. Verhey, R. Poelmann, R. Ramakers, K.W. van Dijk, L. Ham, P. Voshol, L. Havekes, M. Van Eck, J. van der Greef, Metabolomics (liver and blood profiling) in a mouse model in response to fasting: a study of hepatic steatosis, Biochimica et Biophysica Acta (BBA) – Molecular and Cell Biology of Lipids 1771 (2007) 1263–1270.

The American Journal of Pathology, Vol. 179, No. 5, November 2011

DOI: 10.1016/j.ajpath.2011.07.014

Metabolic, Endocrine, and Genitourinary Pathobiology

Melanocortin 4 Receptor–Deficient Mice as a Novel Mouse Model of Nonalcoholic Steatohepatitis

Michiko Itoh,* Takayoshi Suganami,* Nobutaka Nakagawa,* Miyako Tanaka,* Yukio Yamamoto,† Yasutomi Kamei,* Shuji Terai,‡ Isao Sakaida,‡ and Yoshihiro Ogawa*§

From the Department of Molecular Medicine and Metabolism, Medical Top Track Program,† Medical Research Institute, and Global Center of Excellence Program,§ International Research Center for Molecular Science in Tooth and Bone Diseases, Tokyo Medical and Dental University, Tokyo, Japan; and the Department of Gastroenterology and Hepatology,‡ Yamaguchi University Graduate School of Medicine, Yamaguchi, Japan*

Obesity may be viewed as a state of chronic low-grade inflammation that participates in the development of the metabolic syndrome. Nonalcoholic steatohepatitis (NASH) is considered a hepatic phenotype of the metabolic syndrome and a high risk for progression to cirrhosis and hepatocellular carcinoma. Although the "two hit" hypothesis suggests involvement of excessive hepatic lipid accumulation and chronic inflammation, the molecular mechanisms underlying the development of NASH remain unclear, in part because of lack of appropriate animal models. Herein we report that melanocortin 4 receptor–deficient mice (MC4R-KO) develop steatohepatitis when fed a high-fat diet, which is associated with obesity, insulin resistance, and dyslipidemia. Histologic analysis reveals inflammatory cell infiltration, hepatocyte ballooning, and pericellular fibrosis in the liver in MC4R-KO mice. Of note, all of the MC4R-KO mice examined developed well-differentiated hepatocellular carcinoma after being fed a high-fat diet for 1 year. They also demonstrated enhanced adipose tissue inflammation, ie, increased macrophage infiltration and fibrotic changes, which may contribute to excessive lipid accumulation and enhanced fibrosis in the liver. Thus, MC4R-KO mice provide a novel mouse model of NASH with which to investigate the sequence of events that make up diet-induced hepatic steatosis, liver fibrosis, and hepatocellular carcinoma and to aid in understanding the pathogenesis of NASH, pursuing specific biomarkers, and evaluating potential therapeutic strategies. ***(Am J Pathol 2011, 179: 2454–2463; DOI: 10.1016/j.ajpath.2011.07.014)***

Nonalcoholic fatty liver disease (NAFLD) is characterized by increased accumulation of lipids in the liver without a history of excessive alcohol consumption or known liver disease.[1] NAFLD often occurs with the metabolic syndrome, a constellation of visceral fat obesity, impaired glucose metabolism, atherogenic dyslipidemia, and elevated blood pressure, and is considered the hepatic manifestation of the metabolic syndrome.[2] Patients with nonalcoholic steatohepatitis (NASH), a subset of NAFLD, are at high risk for progression to cirrhosis and hepatocellular carcinoma (HCC). However, the molecular mechanisms involved in disease progression from simple steatosis to NASH to HCC are currently unclear. This is in part because there are no appropriate animal models that reflect a liver condition of human NASH, although many attempts have been made to generate animal NASH models via genetic, dietary, and pharmacologic approaches.[3]

The pathogenesis of NASH is thought to involve a multistep process in which the first step is excessive accumulation of lipids in the liver. According to the "two hit" hypothesis, the development of NASH requires the presence of additional pathogenic factors such as oxidative stress, endotoxins, cytokines, chemokines, and lipotoxicity.[4–6] Because NASH is often associated with visceral fat obesity, there should be a mechanistic link

Supported in part by grants-in-aid for scientific research from the Ministry of Education, Culture, Sports, Science, and Technology of Japan, the Ministry of Health, Labour and Welfare of Japan, Japan Science and Technology Agency, and research grants from Takeda Science Foundation, Ono Medical Research Foundation, The Naito Foundation, Yamaguchi Endocrine Research Foundation, and Usage/Research Program of Medical Research Institute, Tokyo Medical and Dental University.

Accepted for publication July 13, 2011.

Supplemental material for this article can be found on *http://ajp.amjpathol.org* or at doi: 10.1016/j.ajpath.2011.07.014.

Address reprint requests to Yoshihiro Ogawa, M.D., Ph.D., or Takayoshi Suganami, M.D., Ph.D., Department of Molecular Medicine and Metabolism, Medical Research Institute, Tokyo Medical and Dental University, 1-5-45 Yushima, Bunkyo-ku, Tokyo 113-8510, Japan. E-mail: ogawa.mmm@mri.tmd.ac.jp or suganami.mmm@mri.tmd.ac.jp.

between the adipose tissue and the liver.[7] Adipose tissue secretes a large number of bioactive substances or adipocytokines such as leptin and adiponectin. Unbalanced production of pro-inflammatory and anti-inflammatory adipocytokines in obesity has been implicated in the pathogenesis of obesity-related complications including NAFLD.[7,8] Indeed, deficiency of leptin signaling protects against hepatic fibrosis in several rodent models of chronic liver injury,[9–11] which suggests that leptin may accelerate development of liver fibrosis. In contrast, studies in adiponectin-deficient mice have revealed that adiponectin is protective against development of hepatic fibrosis and inflammation.[12]

The melanocortin 4 receptor (MC4R) is a seven-transmembrane G protein–coupled receptor that is expressed in the hypothalamic nuclei and is implicated in regulation of food intake and body weight.[13] Previous studies have identified many pathogenic mutations of the *MC4R* gene at a relatively high frequency in severe early-onset obesity, which suggests that *MC4R* mutations are the most common known monogenic cause of obesity in humans.[14] Some leptin biological actions are mediated, at least in part, via the central melanocortin system.[15] Indeed, mice with targeted disruption of *MC4R* have developed late-onset obesity associated with hyperphagia, hyperinsulinemia, and hyperglycemia.[16,17] MC4R-deficient mice (MC4R-KO mice) fed a high-fat diet (HFD) exhibit massive hepatic steatosis and altered gene expression related to lipid metabolism.[18,19] The role of MC4R in the pathogenesis of NASH, however, has not been elucidated.

Herein we report for the first time that MC4R-KO mice develop a liver condition similar to human NASH when fed an HFD, which is associated with obesity, insulin resistance, and dyslipidemia. Of note, they also demonstrate enhanced adipose tissue inflammation, which may contribute to excessive lipid accumulation and enhanced fibrosis in the liver. Moreover, they develop well-differentiated HCC when fed the HFD for a prolonged time. Our data suggest that MC4R-KO mice would provide a novel rodent model of NASH with which to investigate the sequence of events that make up diet-induced hepatic steatosis, liver fibrosis, and HCC.

Materials and Methods

Animals

MC4R-KO mice on the C57BL/6J background were a gift from Dr. Joel K. Elmquist (University of Texas Southwestern Medical Center, Dallas, TX).[13] Male C57BL/6J wild-type (WT) mice were purchased from CLEA Japan, Inc. (Tokyo, Japan). The animals were housed in individual cages in a temperature-, humidity-, and light-controlled room (12-hour light and 12-hour dark cycle) and allowed free access to water and standard diet (CE-2; 343.1 kcal/100 g, 12.6% energy as fat; CLEA Japan, Inc.), unless otherwise noted. In the HFD feeding experiments, 8-week-old male mice were given free access to water and either standard diet or HFD (D12492; 524 kcal/100 g, 60% energy as fat; Research Diets, Inc., New Brunswick, NJ) for 8 or 20 weeks. Detailed dietary composition of the standard diet and HFD is given in Supplemental Table S1 (available on *http://ajp.amjpathol.org*). At the end of the experiments, the animals fed *ad libitum* were sacrificed after administration of 30 mg/kg i.p. pentobarbital anesthesia. All animal experiments were conducted in accordance with the guidelines of the Tokyo Medical and Dental University Committee on Animal Research (No. 100098).

Blood Analysis

Blood glucose concentration was measured using the blood glucose test meter (Glutest PRO R; Sanwa Kagaku Kenkyusho Co., Ltd., Nagoya, Japan). Serum alanine aminotransferase, triglyceride (TG), free fatty acid (FFA), and total cholesterol concentrations were measured using the respective standard enzymatic assays. Serum concentrations of insulin and adipocytokines were determined using the respective enzyme-linked immunosorbent assay kits (insulin, Morinaga Co. Ltd., Tokyo, Japan; adiponectin, Otsuka Pharmaceutical Co., Ltd., Tokyo, Japan; and leptin and IL-6, R&D Systems, Inc., Minneapolis, MN). The homeostasis model assessment insulin resistance index was calculated as [fasting glucose (mg/dL) × fasting insulin (μU/mL)]/405.

Hepatic TG Content

Total lipids in the liver were extracted using ice-cold chloroform and methanol, 2:1 (v/v). TG concentrations were measured using an enzymatic assay kit (Wako Pure Chemical Industries, Ltd., Osaka, Japan).[20]

Histologic Analysis

The liver and epididymal white adipose tissue were fixed with neutral-buffered formalin and embedded in paraffin. Two-micrometer-thick sections of liver were stained using H&E, Masson's trichrome, and Sirius red.[20,21] The presence of α-smooth muscle actin (α-SMA) and α-fetoprotein was detected at immunohistochemistry using mouse monoclonal anti-human α-SMA antibody (Dako A/S, Glostrup, Denmark) and polyclonal goat anti-human α-fetoprotein antibody (Santa Cruz Biotechnology, Inc., Santa Cruz, CA), respectively.[20] Areas positive for Sirius red and α-SMA were measured using WinROOF software (Mitani Corp., Tokyo, Japan). Five-micrometer-thick sections of the epididymal white adipose tissue were stained using anti-mouse F4/80 antibody.[22,23] The number of nuclei surrounded by F4/80-positive cells was counted in a 10 mm^2 area of each section and expressed as the mean per millimeter squared for quantification of F4/80-positive macrophages. Liver histologic features were assessed by two investigators (S.T. and I.S.) who had no knowledge of the origin of the slides according to the NASH clinical research network scoring system.[24] In brief, an NAFLD activity score higher than 5 was considered "definite NASH."[24] The liver fibrosis score was determined semiquantitatively as follows: stage 0, no fibrosis; stage 1,